The Essential Roles of Exosome and CircRNA_101093 to Desensitize Lung Adenocarcinoma to Ferroptosis

Xiao Zhang
Shanghai Chest Hospital: Shanghai Jiao Tong University Affiliated Chest Hospital
Yunhua Xu
Shanghai Chest Hospital: Shanghai Jiao Tong University Affiliated Chest Hospital
Lifang Ma
Shanghai Chest Hospital: Shanghai Jiao Tong University Affiliated Chest Hospital
Keke Yu
Shanghai Chest Hospital: Shanghai Jiao Tong University Affiliated Chest Hospital
Yongjie Niu
Shanghai Municipal Hospital of Traditional Chinese Medicine
Xin Xu
Shanghai Chest Hospital: Shanghai Jiao Tong University Affiliated Chest Hospital
Yi Shi
Shanghai Jiao Tong University School of Medicine
Susu Guo
Shanghai Chest Hospital: Shanghai Jiao Tong University Affiliated Chest Hospital
Xiangfei Xue
Shanghai Tenth People's Hospital
Yikun Wang
Shanghai Chest Hospital: Shanghai Jiao Tong University Affiliated Chest Hospital
Shiyu Qiu
Shanghai Chest Hospital: Shanghai Jiao Tong University Affiliated Chest Hospital
Jiangtao Cui
Shanghai Chest Hospital: Shanghai Jiao Tong University Affiliated Chest Hospital
Hong Wang
Shanghai Jiao Tong University Medical Library: Shanghai Jiao Tong University School of Medicine
Xiaoting Tian
Shanghai Chest Hospital: Shanghai Jiao Tong University Affiliated Chest Hospital
Yayou Miao
Shanghai Chest Hospital: Shanghai Jiao Tong University Affiliated Chest Hospital
Fanyu Meng

Shanghai Chest Hospital: Shanghai Jiao Tong University Affiliated Chest Hospital

Yongxia Qiao

Shanghai Jiao Tong University School of Medicine

Yongchun Yu

Shanghai Chest Hospital: Shanghai Jiao Tong University Affiliated Chest Hospital

Jiayi Wang (karajan2@163.com)

Shanghai Jiao Tong University Affiliated Chest Hospital https://orcid.org/0000-0003-1688-2864

Research

Keywords: exosome, lipid peroxidation, poly-unsaturated fatty acid, taurine and N-Arachidonoyl taurine, RNA-protein interaction

Posted Date: August 31st, 2021

DOI: https://doi.org/10.21203/rs.3.rs-829314/v1

Abstract

Background

Resistance to ferroptosis, a regulated cell death caused by iron-dependent excessive accumulation of lipid peroxides has recently been linked to lung adenocarcinoma (LUAD), the most prevalent lung cancer subtype. Despite intracellular antioxidant system is required for protection against ferroptosis, whether and how extracellular system desensitizes LUAD cells to ferroptosis is incompletely known.

Methods

Immunohistochemistry (IHC) and immunoblotting (IB) were used to analyze protein expression, and quantitative RT-PCR (qPCR) was used to analyze mRNA level. Cell viability, cell death and the lipid reactive oxygen species (ROS) generation were measured to evaluate the responses to ferroptosis induction. Metabolites were measured using appropriate kits. Exosomes were observed using transmission electron microscope (TEM). The localization of arachidonic acid (AA) was detected using click chemistry labeling followed by confocal microscope observation. Interaction between RNA and protein were detected using RNA-pulldown, RNA immunoprecipitation (RIP) and photoactivatable ribonucleoside-enhanced crosslinking and immunoprecipitation (PAR-CLIP). Proteomic analysis was used to investigate circRNA_101093 (cir93) regulated protein and metabolomic analysis was used to analyze metabolites that changed among LUAD tissues expressing low and high Fatty acid-binding protein 3 (FABP3) levels. Cell-derived xenograft (CDX), patient-derived xenograft (PDX) and cell-implanted intrapulmonary LUAD mouse models and plasma/tissue specimens from LUAD patients were used to validate the mechanism that exosome and cir93 desensitized ferroptosis in LUAD.

Results

Here, the roles of exosome and circular RNA (circRNA) to desensitize LUAD cells to ferroptosis were investigated. Plasma exosome from LUAD patients exclusively reduced lipid peroxidation and desensitized ferroptosis. This might because exosomal-cir93 sustained an elevation of intracellular-cir93 in LUAD to modulate AA, a poly-unsaturated fatty acid that is critical for ferroptosis-associated over peroxidation in the plasma membrane. Mechanistically, cir93 interacted and lifted FABP3, which transported and facilitated AA reaction with taurine. Thus, global-AA was reduced while N-Arachidonoyl taurine (NAT), the product of AA and taurine, was induced. Notably, a role of NAT to suppress AA incorporation into plasma membrane was also revealed. In pre-clinical in vivo models, reducing exosome exhibited an improvement of ferroptosis-based treatment.

Conclusion

Exosome and cir93 are essential for desensitizing LUAD cells to ferroptosis, and blocking exosome will be helpful for future LUAD treatment.

Background

Lung cancer is one of the leading causes of malignant death worldwide, with lung adenocarcinoma (LUAD) being the most prevalent subtype [1]. Although driver mutations such as those in epidermal growth factor receptor (EGFR), v-Ki-ras2 Kirsten rat sarcoma viral oncogene homolog (kRAS), anaplastic lymphoma kinase (ALK) and tumor protein 53 (p53) are major causes of LUAD [2, 3], other mechanism, for example, dysregulation of N^6-methyladenosine (m^6A) RNA methylation is still critical for LUAD tumorigenesis [4, 5]. Recently, resistance to ferroptosis, a newly identified regulated cell death caused by iron-dependent excessive accumulation of lipid peroxides, has been regarded as another non-mutation mechanism linked to initiation and progression of LUAD [5-7]. Although a higher-than-normal-cell metabolic activity enables tumor cells to produce more lipid peroxides [8], the existence of intracellular anti-oxidant system strongly protects LUAD cells against ferroptosis [4, 5, 7]. However, whether and how extracellular system also desensitizes LUAD cells to ferroptosis still remains unclear.

Exosome is a type of extracellular vesicle that originated from endocytosis [9]. As a master regulator of cellular signaling, exosome orchestrates various autocrine and paracrine functions to alter tumor micro-environment, growth and progression [10]. Reasoning that exosome can not only be taken by target cells but also secreted from host cells, they are critical messengers participating in cell-to-cell communications [11]. Interestingly, one exciting study has revealed that ferroptosis-resistance in tumor cells is achieved by formation of ferritin-containing exosome that takes labile iron out of the cell [12]. However, what are the effects on the sensitivity of LUAD cells to ferroptosis following uptake of extracellular exosome have not been explained yet.

Besides metabolite like iron, circular RNAs (circRNAs) are also important contents in exosome [13]. Increasing studies have demonstrated that circRNAs are closely linked to LUAD tumorigenesis [14]. CircRNAs are more stable than other kinds of RNAs because of their covalently closed loop structure [15]. The protection of the vesicles further increases stability of circRNAs and makes them more efficient to transmit information among cells [16]. However, our knowledge understanding the roles of circRNAs in modulating sensitivity of LUAD cells to ferroptosis is still quite limited.

Despite the functions of circRNAs as competing endogenous RNAs (ceRNAs) are well established, the roles of circRNAs to interact with proteins are less understood [17]. Reasoning that ferroptosis is closely associated with metabolism [18], those proteins exerting dual-roles in interacting with circRNAs and participating in metabolism could be strong candidates to influence ferroptosis. Fatty acid-binding proteins (FABPs) are critical for the transport of poly-unsaturated fatty acids (PUFA) to specific cellular compartments [19]. Notably, peroxidation of PUFA, mainly arachidonic acid (AA) and adrenal acid (AdA) in the plasma membrane, are essential for sensitizing cells to ferroptosis [20]. However, whether and how circRNA-FABPs interactions regulate PUFA and ferroptosis sensitivity remains largely unknown.

Therefore, the aim of the present study was to investigate whether and how exosome and circRNA desensitize LUAD cells to ferroptosis. We uncovered that exosomal-cir93 is critical for elevating

intracellular-cir93 in the tumor part of LUAD, by which eventually upregulates intracellular Fatty acid-binding protein 3 (FABP3). FABP3 facilitates AA reaction with taurine and thus reduces global-AA. In addition, N-Arachidonoyl taurine (NAT), the product of taurine and AA, also suppresses AA incorporation into the plasma membrane. Thus, the opportunity for lipid peroxidation and followed ferroptosis is mitigated in LUAD.

Materials And Methods

Cell culture

Established MRC-5, WI38, H358, H1650, PC9, H1975, A549 and H1299 cell lines were purchased from Fuheng Biotechnology (Shanghai, China) and validated by short tandem repeat analysis. For monolayer culture, cells were cultured with Dulbecco's modified eagle medium (DMEM) supplemented with 10% fetal bovine serum (FBS) and 1% penicillin/streptomycin. Patient-derived primary LUAD cells were derived from LUAD tissues. Briefly, fresh LUAD tissues without necrosis were washed with ice-cold Dulbecco's phosphate buffered saline (DPBS) for 3 times before re-suspending in DMEM containing collagenase I (2 mg/ml, Solarbio, Shanghai, China) at 37 °C, 5%CO_2 for 4 h. After washing for 3 additional times with fresh DMEM, cells were cultured in routine conditions for 1 week. Subsequently, tumor epithelial cells were sorted using anti-epithelial cell adhesion molecule (EpCAM) antibodies (R&D systems, Minneapolis, MN, USA, #FAB9601G) by a flow cytometer, thus the EpCAM (+) cells were obtained, and the left cells were regarded as EpCAM (-) cells. For 3D spheroid culture, basement membrane extract (BME) (Trevigen, Gaithersburg, MD, USA) was seeded in a 96-well plate at 50 μl/well and plated at 37 °C for 30 min. Then, cells were seeded on top of BME at a density of 1×10^5 cells per well. After formation of spheroids, they were treated with dimethyl sulfoxide (DMSO), erastin (Sigma, St Louis, MO, USA) or ras-selective lethal small molecule 3 (RSL3, Sigma). Images were captured after staining with SYTOX green (Invitrogen, Carbsland, CA, USA).

Mouse experiments and patient information

For generations of routine cell-derived xenograft (CDX) mouse models, established LUAD cells (initial $5x10^6$) were subcutaneously injected into 6-week-old athymic nude mice (Jiesijie, Shanghai, China). For generation of H1975/A549 cell-implanted intrapulmonary LUAD mice, 6-week-old athymic nude mice were intrapulmonarily injected with cells ($5x10^6$) under anesthesia prior to intranasal administrating with AAV5 particles ($2x10^{12}$ viral particles/ml, Genomeditech, Shanghai, China) 3 weeks later. For generation of patient-derived xenograft (PDX) mouse models, fresh LUAD tissues in a size of 2-3 mm^3 were subcutaneously implanted into six-week-old athymic nude mice. After successful passage, the PDX mice were used for further study. Tumor volumes were calculated as $0.5 \times L \times W^2$ (L indicating length while W indicating width). For drug administration, piperazine erastin (PKE, MedChemExpress, Monmouth Junction, NJ, USA) and GW4869 (Sigma) were injected.

The basic patient information for Fig. 1A and C, 2B-C and 7A-C, and Supplementary Fig. S1A-B, S2A-B and S7A were summarized in Supplementary Table. S1. The information for Fig. 1B were summarized in Supplementary Table. S2. The information for healthy individuals and LUAD patients in Fig. 1E-F, 2D, 4M, 5H-I, 1G, 6F and 6N, are available in Supplementary Table. S3, S4 and S5. Also, the information for Fig. 2E, 7D-E, 4I, 7J and Supplementary Fig. S7B-C was summarized in Supplementary Table. S6, S7, S8 and S9. All the tissue and plasma specimens were recruited in Shanghai Chest Hospital (Shanghai, China) from May 2013 to December 2020. Mutations in tissues were sequenced by Mapbioo Biotechnology (Shanghai, China). All the informed written consents were obtained. The study including those for animals were approved by the institutional ethics committee of Shanghai Chest Hospital.

Reagents and plasmids

For reagents, erastin (Sigma), RSL3 (Sigma), GW4869 (Sigma), 5,5-(N-N-dimethyl)-amiloride hydrochloride (DMA, Sigma), deferoxamine (DFO, Sigma), Ferrostatin-1 (Fer-1, Sigma), NAT (Cayman, Ann Arbor, MI, USA), Actinomycin D (ActD, Sigma), C11-BODIPY$^{581/591}$ (Invitrogen), propidium iodide (PI, Sigma) were used for cell treatments.

For plasmids, WT and mutant-circRNA_101093 (cir93, including cir93$^{\triangle R\#1}$, cir93$^{\triangle R\#2}$) expressing plasmids were purchased from Geneseed Biotechnology (Guangzhou, Gongdong Province, China). Anti-cir93-1/2 plasmids were purchased from Sangon (Shanghai, China). WT-FABP3 expressing plasmids were purchased from Biovision (Shanghai, China). Plasmids expressing mutant-FABP3 including FABP3$^{\triangle P\#1}$, FABP3$^{\triangle P\#2}$, FABP3$^{\triangle P\#3}$, FABP3$^{\triangle P\#4}$ and FABP3^{F16S} were constructed using overlapping PCR and cloned into pcDNA3.1(+) plasmids. LentiCRISPR v2-based constructs were used for knockout of FABP3. shRNAs targeting against cysteine sulfinic acid decarboxylase (CSAD) and cysteine dioxygenase type 1 (CDO1) were purchased from Biovision. The sequences for primers, gRNAs and shRNAs were summarized in Supplementary Table S10.

Immunofluorescence (IF), immunohistochemistry (IHC), immunoblotting (IB) and enzyme linked immunosorbent assay (ELISA)

IF, IHC and IB were performed as per conventional protocols. For IF, PKH67 (Sigma, MKCG5294) was probed for marking exosome packaged in A549/H1299 cells. For IHC, the primary antibodies used in the study were, anti-alpha smooth muscle actin (αSMA, Abcam, Hong Kong, China, #ab7817) and anti-4-hydroxynonenal (4-HNE, Abcam, #ab48506). For IB, the primary antibodies used were, anti-FABP3 (Abcam, #ab133585), anti-GAPDH (Abcam, #ab181602), anti-CSAD (Abcam, #ab91016), anti-CDO1 (Abcam, #232699), anti-acyl-CoA synthetase long-chain family member (ACSL4, Abcam, #ab155282), anti-lysophosphatidylcholine acyltransferase 3 (LPCAT3, Abcam, #ab232958), anti-phospholipid transfer protein (PLTP, Abcam, #ab134066), anti-Myc (CST, #2276), anti-cluster of differentiation 63 (CD63, Abcam, #ab271286), anti-tumor susceptibility 101 (TSG101, Abcam, #125011), anti-ALG-2 interacting protein X (ALIX, Abcam, #ab275377), anti-cluster of differentiation 9 (CD9, Abcam, #ab92726) and anti-Calnexin (Abcam, #ab133615). For ELISA, FABP3, hepatocyte nuclear factor alpha (HNF4a) and

hypermethylated in cancer 1 (HIC1) levels were measured using kits from Yingxin Biotech Ltd. (Shanghai, China) as per manufacturer's instructions.

Measurements of metabolites

AA was measured using a kit from CUSABIO (Houston, TX, USA), malondialdehyde (MDA) and taurine were measured using kits from Abcam according to the manufacturer's instructions. NAT was analyzed by HPLC-ESI-MS/MS. The high performance liquid chromatograph (HPLC) system was Agilent 1100 (Agilent, Chandler, Arizona, USA). Mass spectrometry (MS) system was AB 6500+ triple quadrupole tandem MS detection system (AB Sciex, Boston, MA, USA) equipped with electrospray ionization (ESI) source and Analyst 1.7.1 workstation.

Quantitative RT-PCR (qPCR)

Total RNA was extracted using Trizol reagent (Ambion, Carlsbad, CA, USA) and reverse-transcribed into cDNA using the PrimeScriptTM RT reagent kit (Takara, Dalian, China). For real-time qPCR, the SYBR premix Ex Taq (Takara) kit was used for detecting the relative levels of *Nucleoporin 107 (NUP107)* mRNA, cir93 and circRNA_100934 (cir34). Semi-qPCR was also performed to examine *NUP107* mRNA and cir93, and the reaction was terminated at the cycle 29 and the products were visualized by agarose gel electrophoresis. The primers are listed in Supplementary Table S10.

Measurements of cell viability, cell death, lipid reactive oxygen species (ROS) generation and ex vivo tissue slice culture

Cell viability was detected using a CellTiter-Glo luminescent cell viability assay kit (Promega, Madison, WI, USA). Cell death was measured by staining with SYTOX Green followed by flow cytometry. Lipid ROS generation was analyzed by probing with C11-BODIPY$^{581/591}$ at a final concentration of 1.5 μM for 20 min before subjecting for further analysis using flow cytometer. For ex vivo tissue slices, they were prepared through a similar protocol described in our previous study [21]. Afterwards, DMSO, erastin or Fer-1 was co-incubated before tissue slices were stained with PI and photographed under microscope.

Transmission electron microscope (TEM) analysis

For exosome observation, exosome was resuspended in 4% paraformaldehyde (PFA), and images were captured using the JEM1230 TEM (JEOL, Tokyo, Japan). For morphological observation of mitochondria, cells were seeded onto 4-well chambered cover glass (Thermo Scientific, Waltham, MA, USA) at a density of 15,000 cell/well. Images were captured using the Olympus EM208S TEM (HITACHI, Tokyo, Japan).

Fluorescence in situ hybridization (FISH)

The main procedure was similar with that of conventional IHC but with several additional steps before adding primary antibodies. Briefly, tissues were incubated by a formamide/saline sodium citrate (SSC) solution at 37 ℃ for 4 h prior to the addition of digoxigenin (DIG)-labeled cir93 or cir34 probes (Sangon,

Shanghai, China, listed in Supplementary Table S10) at 37 ℃ overnight. Afterwards, the primary anti-DIG antibodies (Abcam, #ab420) and HRP-labeled secondary antibodies (CST) were used for final visualization of cir93 and cir34.

Isolation and measurement of exosome

Exosome was isolated from cultured media of cells or plasma of human via three sequential centrifugation steps at 4 ℃, 1) 15 min at 500g to remove cells; 2) 30 min at 10,000g to remove cell debris; and 3) ultracentrifugation at 110,000g for 70 min to pellet exosome. The pellet was finally re-suspended in PBS and centrifuged at 110,000g for another 70 min to remove soluble and secreted proteins. The concentration and size of exosome were analyzed using a Nanosight NS 300 system (NanoSight Technology, Malvern, UK).

Click chemistry for alkyne labeling

Cells were incubated with DMEM containing 10% FBS, 3% BSA ± AA-alkyne or AdA-alkyne (20 mM, Wuxi AppTec, Wuxi, China) for 2 h. Next, the treatment medium was replaced by fresh DMEM containing 3% BSA for another 10 h and cells were subsequently fixed in 4% PFA and permeabilized with 0.1% Triton-X in PBS. Afterwards, cells were incubated with the PBS-based click reaction buffer [0.1 mM Azide-fluor 488 (Cat# 760765, Sigma), 1 mM $CuSO_4$, 1 mM TCEP] for 1 h in a light-impermeable humid chamber. Finally, cells were washed 5 times with 1x PBS and blocked with PBS-BT (1x PBS, 3% BSA, 0.1% Triton X-100, 0.02% NaN_3) for 45 min at RT followed by probing with Concanavalin A-Alexa Fluor 350 and DAPI (Molecular Probes, Eugene, OR, USA). Images were captured using a confocal microscope.

RNA pull-down, RNA immunoprecipitation (RIP) and photoactivatable ribonucleoside-enhanced crosslinking and immunoprecipitation (PAR-CLIP)

For RNA pull-down assay, synthesized cir93 (including WT and mutants) and its antisense probes were labeled with biotin and ordered from Sangon (listed in Supplementary Table S10). About 1×10^7 cells were lysed and incubated with 3 μg biotinylated probes at 4℃ overnight. The biotin-coupled RNA-protein complex was pull-downed with streptavidin magnetic beads (Life Technologies, Carlsbad, CA, USA) for another 4 h. After washing for five times with PBS, the streptavidin beads were boiled and the elutes were subjected for IB or proteomic analysis.

For RIP assay, a Magna RIP Kit (Merck Millipore, Billerica, MA, USA) was used. Briefly, cell lysates were incubated with magnetic beads loaded with 5 μg anti-FABP3 antibodies (Abcam, #ab133585) or control IgG (CST #3900) overnight at 4 ℃. The remaining RNA after proteinase K digestion was extracted by TRIzol regent and analyzed by qPCR.

For PAR-CLIP, cells were incubated with 4-SU (250 μM, Sigma) for 16 h followed by irradiation with 365 nm UV light for crosslinking. Subsequently, cells were lysed with NP40 lysis buffer on ice and centrifuged at 18,000g for 15 min to collect supernatant, which was further incubated with 600 μl protein A

dynabeads (Invitrogen) bound with 15 μg anti-FABP3 antibodies (Abcam, #ab133585) for 2 h. After washing three times with IP wash buffer, beads were re-suspended and boiled at 95 ℃ for 10 min. To detect FABP3-bound circRNAs, RNA was recovered and subjected into qPCR analysis.

Proteomic and metabolomic analysis

Proteomic and metabolomic analysis were performed and analyzed by Luming Biotechnology (Shanghai, China). The data of proteomics regarding the proteins that controlled and pulled down by cir93 have been deposited in ProteomeXchange Consortium.

Statistical analysis

Tests used to examine the differences between groups were student's t test, one-way, two-way ANOVA and χ^2 test. The correlation between two groups was evaluated by the Spearman rank-correlation analysis. The survival rate was calculated by Kaplan-Meier method and statistical significance was assessed by log-rank tests. A $P< 0.05$ was considered statistically significant.

Results

Exosome antagonized lipid peroxidation and desensitized ferroptosis in LUAD

Excessive lipid peroxidation is a hallmark of ferroptosis, and HNF4a and HIC1 play opposite roles in ferroptosis [22]. MDA, a byproduct of lipid peroxidation, was anti-correlated with anti-ferroptotic HNF4a, while was correlated with pro-ferroptotic HIC1 in LUAD (Supplementary Fig. S1A-B), confirming that MDA reflects ferroptosis-associated lipid peroxidation.

We were curious to know whether lipid peroxidation is suppressed in LUAD, and indeed, MDA levels were lower in LUAD tissues in comparison to the matched adjacent tissues (Fig. 1A). In addition, 39.9% LUADs (75/188) also showed downregulation of 4-HNE, another byproduct of lipid peroxidation in LUAD (Fig. 1B). As known, LUADs are commonly driven by mutations [2, 3]; however, after screening common mutations within EGFR (Del19, L858R and T790M), kRAS (G12C, G12S, G12A and G13C) and p53 (R196P, H179Y, P250L, R249S and R248G), we found that MDA at least might not be determined by these driver mutations (Fig. 1C). Collectively, lipid peroxidation is suppressed possibly via a driver mutation-independent manner in a large proportion of LUAD.

Then, we tested whether exosome suppresses lipid peroxidation and desensitizes LUAD cells to ferroptosis. Ex vivo primary LUADs from patients for curative therapy were treated with or without GW4869 and DMA, two exosome biogenesis inhibitors, and they both elevated 4-HNE (Fig. 1D), hinting that prevention of exosome generation stimulates lipid peroxidation. Does exosome from LUAD plasma desensitize ferroptosis? To this end, plasma exosome from healthy individuals and LUAD patients were extracted and verified by TEM (Fig. 1E). The exosome diameters were mainly between 30 and 150 nm (Supplementary Fig. S1C), which were similar to that reported in prior studies [23, 24]. Except

endoplasmic reticulum (ER) biomarker Calnexin, exosome biomarkers including CD63, TSG101, ALIX and CD9 were all clearly detected in our samples (Supplementary Fig. S1D), further demonstrating the quality of the exosome. A549 and H1975 LUAD cell lines were picked up for further study because they exhibited the least and the most sensitivity to erastin and RSL3, two ferroptosis agonists, among the LUAD cell lines tested in 3D spheroid culture (Supplementary Fig. S1E-F). By pre-co-incubating H1975 cells with exosome, we found that plasma exosome from a large proportion of LUAD patients could significantly prevent erastin- and RSL3-reduced cell viability and -induced cell death and lipid ROS generation. By comparison, plasma exosome from healthy individuals failed to do so (Fig. 1F). The results from 3D spheroid culture, which is a better way to reflect cell-cell interaction than monolayer culture, also supported that only the exosome from LUAD plasma had the capacity to prevent erastin- and RSL3-induced cell death in H1975 spheroids (Fig. 1G). Reasoning that the sensitivity to ferroptosis was varied between A549 and H1975 cells, we wondered whether the exosome from A549 cells was required for H1975 cells to obtain a less sensitivity to ferroptosis. As expected, pre-co-incubation with exosome that extracted from A549-cultured DMEM or directly the DMEM itself desensitized H1975 cells to the induction of erastin and RSL3 (Fig. 1H). However, fresh DMEM, DMEM from cultured H1975 cells and A549 cells following GW4869 treatment did not have such effects (Fig. 1H). Together, a role of exosome to antagonize lipid peroxidation and desensitize LUAD cells to ferroptosis was established.

A link between exosomal- and intracellular-cir93 in LUAD

Then, important contents in the exosome were investigated. Emerging studies have demonstrated the critical roles of exosomal-circRNAs in tumorigenesis [25, 26]; we thereby tried to identify such circRNAs in LUAD exosome. Firstly, the available circRNA-chip data (Zhu, et al., Ref. 27 and Yang, et al., GSE101586) evaluating differential circRNA expression between LUAD and normal lung were mined. Two circRNAs, i.e. cir93 and cir34 were identified as the common upregulated intracellular-circRNAs in LUAD between the two datasets (Fig. 2A). Further verifications indicated that only cir93, but not cir34 was elevated in our LUAD cohort (n=250, Fig. 2B-C and Supplementary Fig. S2A-B), and this led us to focus on cir93 hereafter. Dislike *NUP107* mRNA, the transcript of cir93 parental gene, cir93 could only be PCR amplified from cDNA but not gDNA template of A549 and H1299 cells using circRNA-specific primer sets (Supplementary Fig. S2C), suggesting that cir93 is a genuine circRNA. Of note, an elevation of plasma exosomal-cir93 was also observed in LUAD (n=200) as compared to healthy individuals (n=200, Fig. 2D). Reasoning that circRNA can be transmitted via exosome between host and target cells [28], we suggested that elevation of intracellular-cir93 is closely linked with exosomal-cir93 in LUAD.

Exosome secreted by tumor cells themselves was essential for elevating intracellular-cir93 in LUAD

Because tumor and tumor stroma are both important for tumorigenesis [29, 30], we thereby wanted to ascertain whether they are involved separately or in combined for the link between exosomal- and intracellular-cir93. After measuring cir93 in LUAD tissue specimens, we found 68.0% of them (34/50) exclusively expressing cir93 in the tumor part. By contrast, only 4.0% (2/50) exhibited an exclusive cir93 expression in the stroma part (Fig. 2E). Those specimens with cir93 exclusively expressed in tumor part

were further evaluated by IHC using antibodies against αSMA; a biomarker of fibroblast and to some extent capable of distinguishing stroma from tumor parts. Indeed, all of them (34/34) showed mutual exclusion of cir93 and αSMA within the same areas (Fig. 2F). EpCAM is a surface pan-carcinoma antigen. By sorting patient-derived EpCAM (+) and EpCAM (-) cells in primary tumors from 3 distinct LUAD patients, we found that intracellular-cir93 was much higher in EpCAM (+) cells than that in EpCAM (-) cells (Fig. 2G). Taken together, tumor part is the more likely site to establish the link between exosomal- and intracellular-cir93 in LUAD.

Subsequently, we tried to investigate whether exosome secreted by tumor cells themselves elevates intracellular-cir93 in the tumor part of LUAD. To this end, primary EpCAM (+) and EpCAM (-) cells from case #1 and #2 in Fig. 2G were used for further analysis. Before co-incubating cultured-DMEM from the first cells with the secondary cells, the exosome concentrations in cultured DMEM were ensured to be similar between EpCAM (+) and EpCAM (-) cells (Fig. 2H, lanes, 1-4); however, intracellular-cir93 in case #2 EpCAM (+) cells could only be sustained after co-incubating with the cultured-DMEM from case #1 EpCAM (+) cells, and vice versa (Fig. 2H, lanes, 1-2). By contrast, in both case #1 and #2, co-incubation of cultured-DMEM from EpCAM (-) cells failed to sustain intracellular-cir93 in EpCAM (+) cells (Fig. 2H, lanes, 3-4). The critical roles of exosome in EpCAM (+) cells were further verified because reduction of exosome in the cultured-DMEM of the first EpCAM (+) cells following GW4869 treatment failed to sustain intracellular-cir93 in the secondary EpCAM (+) cells (Fig. 2H, lanes, 5-6). In addition to the DMEM, the results from extracted exosome also demonstrated that only that exosome from EpCAM (+) but not EpCAM (-) cells had the capacity to elevate intracellular-cir93 in EpCAM (+) cells (Fig. 2I-J). The valid exosome-mediated cir93 transmission between A549 and H1299 cells was further confirmed by incubating one cell line with extracted PKH67-marked exosome from another cell line expressing mCherry-labeled cir93 followed by tracing the exosome (green) and cir93 (red) under microscope (Fig. 2K). Together, exosome secreted by tumor cells themselves is essential for elevating intracellular-cir93 in the tumor part of LUAD.

Elevated intracellular-cir93 desensitized LUAD cells to ferroptosis via regulating AA

Despite elevation of intracellular-cir93 is sustained by exosome in LUAD (Fig. 2), whether exosome antagonizes ferroptosis via elevating intracellular-cir93 remains unclear. Ferroptosis is characterized by the presence of smaller than normal mitochondria with condensed densities of mitochondrial membrane [31]. Expectedly, treating H1975 cells with erastin and RSL3 resulted in such effects; however, they were prevented by overexpressing cir93 (Fig. 3A). By pre-infecting H1975 cells with dual-cir93 and GFP-expressing lenti-virus and staining the cells with PI, a small fluorescent molecule that binds to DNA but cannot penetrate into live cells, elevating cir93 was also revealed to prevent erastin- and RSL3-induced cell death (Fig. 3B). In addition, like ferroptosis inhibitors Fer-1 and DFO, overexpressing cir93 was capable of holding back erastin- and RSL3-induced reduction of cell viability and induction of lipid ROS generation in H1975 cells (Fig. 3C and Supplementary Fig. 3A). Interestingly, cir93 itself could not be affected by erastin and RSL3 (Supplementary Fig. S3B), suggesting that cir93 is an independent factor to influence ferroptosis. If cir93 truly desensitizes LUAD cells to ferroptosis, anti-cir93 could exert opposite

function. Expectedly, administrating anti-cir93 downregulated intracellular-cir93 in A549 cells (Supplementary Fig. S3C), and aggravated erastin- and RSL3-induced reduction of cell viability and induction of cell death and lipid ROS generation (Supplementary Fig. S3D-F). Thus, the above data demonstrated a role of elevating cir93 to mitigate ferroptosis in vitro.

To investigate whether elevating intracellular-cir93 also desensitizes LUAD cells to ferroptosis in vivo, H1975 cell-implanted intrapulmonary LUAD-bearing mice were intranasal infected with adeno-associated virus 5 (AAV5) dual-expressing cir93 and GFP before further administrating with PKE, an in vivo stable erastin derivative. Compared to the control, cir93 was indeed overexpressed, and PKE-induced elevation of 4-HNE and MDA were largely prevented in intrapulmonary LUAD (Fig. 3D), suggesting that elevating cir93 suppresses ferroptosis-associated lipid peroxidation in vivo. To further investigate whether anti-cir93 oppositely stimulates lipid peroxidation within plasma membrane fraction in mouse LUAD, a fluorescent probe C11-BODIPY$^{581/591}$ was used to directly measure oxidized lipid and conA-AlexaF was employed to visualize membrane. Images were captured at emission at 580/600 nm (the non-oxidized form, red) and 490/510 nm (the oxidized form, green) and then merged to demonstrate the fraction of the oxidized C11-BODIPY$^{581/591}$. As shown in Fig. 3E, the fraction of oxidized C11-BODIPY$^{581/591}$ (green) within the plasma membrane was remarkably increased following administrating with anti-cir93. Combined with the data showing that overexpressing cir93 desensitizes cells to ferroptosis that induced by both erastin and RSL3 (Fig. 3A-C), and reasoning that treating two small molecules both lead to lipid peroxidation [32], we supposed that elevating intracellular-cir93 might desensitize LUAD cells to ferroptosis via suppressing lipid peroxidation.

Next, we investigated how elevating intracellular-cir93 suppresses lipid peroxidation in LUAD cells. Excessive peroxidation of PUFA, such as AA and AdA are prerequisite for the trigger of ferroptosis [20]. Plasma membrane incorporation of AA is also essential for such a process [33]. By a click chemistry-based method using alkyne-labeled AA or AdA and Fluro-488-labeled Azide, we found that elevating cir93 in H1975 cells was capable of reducing AA but not AdA incorporation into the plasma membrane (Fig. 3F-G and Supplementary Fig. S3G-H). Moreover, global-AA could be simultaneously reduced by overexpressing cir93 in H1975 cells (Fig. 5E and 5G). These results suggested that suppression of lipid peroxidation by elevating cir93 might be conducted by modulation of AA.

Finally, we examined whether exosome suppresses lipid peroxidation in a cir93-dependent way. Reasoning that MRC-5 and WI-38, two established lung fibroblasts, demonstrated remarkable lower levels of intracellular-cir93 and exosomal-cir93 in cultured DMEM than LUAD cell lines (Supplementary Fig. S3I), we compared the effects of extracted exosome from MRC-5, WI-38 and LUAD A549 cells on lipid ROS generation following erastin treatment in H1975 cells. We noticed that only exosome from A549 cells significantly reduced lipid ROS generation that induced by erastin (Fig. 3H), hinting that the role of exosome to suppress lipid peroxidation in LUAD cells is via a cir93-dependent way.

FABP3 worked as a downstream of cir93, interacting and being upregulated by cir93

Then, the downstream effectors of cir93 were further investigated. CircRNAs interact with proteins [34, 35]; we hence performed proteomics to seek potential proteins that cir93 might influence. Via pull-down experiments with cir93, anti-sense cir93, or without RNA (blank) followed by proteomics, 143 proteins were identified specifically interacted with cir93 (Fig. 4A). To narrow candidates, we wanted to know which proteins are also cir93-regulated. Because intracellular-cir93 was higher in A549 cells than H1975 cells (Supplementary Fig. S3I), we inhibited cir93 in A549 cells while overexpressed cir93 in H1975 cells before subjecting samples into proteomics again. Only FABP3 was identified upregulated by cir93. Unfortunately, no proteins were identified downregulated by cir93. Interestingly, FABP3 was also one of those 143 proteins interacting with cir93 (Fig. 4A). The upregulation of FABP3 by cir93 was further verified by IB (Fig. 4B). Like cir93, FABP3 could not be regulated by erastin and RSL3 (Fig. 4C and Supplementary Fig. S3B), indicating that FABP3 is also an independent factor to influence ferroptosis. Moreover, elevating cir93-desensitized LUAD cells to erastin- and RSL3-induced ferroptosis and ferroptosis-associated lipid ROS generation were all indispensable of FABP3, because compared to *WT* H1975 cells, cir93 was ineffective in *FABP3*$^{-/-}$ cells (Fig. 4C and Supplementary Fig. S4A-C). Together, FABP3 interacts and being upregulated by cir93, through which facilitates FABP3 working as a downstream of cir93 to desensitize LUAD cells to ferroptosis.

Molecular basis behind cir93-FABP3 interaction and its essential role in modulating FABP3, AA, lipid peroxidation and sensitivity of LUAD cells to ferroptosis

Subsequently, we investigated the molecular basis for cir93 to interact and upregulate FABP3. To further verify that FABP3 interacts with cir93, PAR-CLIP was performed, and we found that FABP3 did not interact with cir34, but rather, interacted with cir93 (Supplementary Fig. S4D). Molecular basis between FABP3 and cir93 was then predicated by catRAPID online software. Three regions, named as P#1 (26^{th}~77^{th} a.a), P#2 (44^{th}~95^{th} a.a) and P#3 (51^{st}~102^{rd} a.a) located within FABP3, and two regions, named as R#1 (57^{th}~108^{th} nt) and R#2 (151^{st} ~202^{rd} nt) located within cir93 were predicted with interaction potentials (Fig. 4D and Supplementary Fig. S4E). Cir93 pull-down experiments demonstrated that deletion of the R#2 region of cir93 exclusively abolished cir93-FABP3 interactions in H1975 cells (Fig. 4E). Reconstitution of *FABP3*$^{-/-}$ H1975 cells by Myc-tagged WT or FABP3 without P#3 region followed by RIP experiments using anti-Myc antibodies indicated that the P#3 region of FABP3 contains critical domain responsible for the cir93-FABP3 interaction (Fig. 4F). The P#1 and P#2 regions of FABP3 were excluded because FABP3 still interacted with cir93 even when they were deleted (Supplementary Fig. S4F). Because P#1, P#2 and P#3 have overlapped regions and only the region compassing 96^{th}~102^{rd} a.a in P#3 is unique as compared to P#1 and P#2 (Fig. 4D), we speculated participation of this region (hereafter named as P#4) in the cir93-FABP3 interaction, and expectedly, deletion of P#4 disrupted cir93-FABP3 interaction in H1975 cells (Fig. 4F). Furthermore, besides P#3, P#4 was also prerequisite for cir93 to upregulate FABP3 (Supplementary Fig. S4G). Together, the molecular basis for cir93-FABP3 interaction and its essential roles to upregulate FABP3 in LUAD cells was elucidated.

Does cir93-FABP3 interaction also influence AA, lipid peroxidation and sensitivity of LUAD cells to ferroptosis? Like elevating cir93, overexpressing FABP3 reduced AA but not AdA incorporation into the plasma membrane of H1975 cells; however, the effects no longer exist once upon the P#4 site was deleted. Deletion of the R#2 region also prevented the roles of cir93 to suppress AA membrane incorporation (Fig. 3F, 4G and Supplementary Fig. S4H-I). Data from Fig. 4H further demonstrated that the cir93-FABP3 interaction was required for the reduction of global-AA (Fig. 4H). To get clinical support, intracellular-cir93 and the open reading frame (ORF) of FABP3 in 30 randomly chosen LUAD tissue specimens were sequenced. Only one specimen (3.3%, 1/30) each contained a mutation in R#2 of cir93 and P#4 of FABP3, respectively (Fig. 4I). The disruption of cir93-FABP3 interaction resulted by the two mutations were subsequently verified (Supplementary Fig. S4J-K). Of note, mutations in cir93 and FABP3 increased 4-HNE concentrations in LUAD (Fig. 4J), further confirming the importance of cir93-FABP3 interaction in reducing lipid peroxidation. Moreover, disruption of cir93-FABP3 interaction abolished the effects of cir93 and FABP3 to desensitize H1975 cells to erastin- and RSL3-induced cell death (Fig. 4K). Collectively, cir93-FABP3 interaction and its role to upregulate FABP3 are essential for modulating AA and reducing lipid peroxidation and sensitivity of LUAD cells to ferroptosis.

Exosome functioned to upregulate FABP3 via the cir93-FABP3 interaction in LUAD

Because the cir93-FABP3 interaction is required for cir93 to upregulate FABP3 (Fig. 4B and Supplementary Fig. S4G), and exosome is essential for elevating intracellular-cir93 in LUAD (Fig. 2); we wondered whether plasma exosome from LUAD lifts intracellular FABP3 expression via the cir93-FABP3 interaction. To address this, plasma exosome from LUAD (n=200) was co-incubated with engineered H1975 cells expressing WT or FABP3 without P#4 region. More than two-fold upregulation of FABP3 in $FABP3^{WT}$-expressing H1975 cells was observed following co-incubation of 68.5% (137/200) exosome, while only 3.5% (7/200) exosome exhibited similar functions in those cells expressing $FABP3^{\triangle P\#4}$ (Fig. 4L-M), suggesting the cir93-FABP3 interaction is also the basis for exosome to upregulate FABP3 in LUAD.

Taurine was essential for cir93-mediated upregulation of FABP3 to modulate AA and desensitize LUAD cells to ferroptosis

Next, we investigated the outcome following upregulation of FABP3 in LUAD. Because FABP3 acts as a transporter responsible for transporting AA to the location where it can react with other metabolites [36, 37], the metabolites both regulated by FABP3 and associated with AA could determine sensitivity of LUAD cells to ferroptosis. To figure out such metabolites, metabolomics were performed to compare metabolites in LUAD tissues expressing high and low levels of FABP3. Among 362 metabolites, 63 were upregulated while 26 were downregulated in FABP3 high-expressing LUADs (n=30) in comparison to the low-expressing ones (n=30, Fig. 5A and Supplementary Fig. S5A). To the best of our knowledge, among all the identified metabolites, taurine was the only one that can also react with AA to generate NAT (Fig. 5A-B and Ref. 38). Because taurine and AA are substrates while NAT are products of this reaction (illustrated in Fig. 5B), a reduction of taurine in FABP3 high-expressing LUAD (Fig. 5A) might be explained

by FABP3-mediated acceleration of the reaction. Unfortunately, a decrease of global-AA and an increase of NAT were not detected by metabolomics, which may due to the methodology limitation [39]. However, after evaluated by ELISA and targeted MS, we found that global-AA and NAT were indeed reduced and induced following overexpressing FABP3 in H1975 cells (Supplementary Fig. S5B-C). FABP3 transports AA via its phenylalanine (F)16 residue [37], we hence replaced this F by a serine (S) to test whether reduction of taurine is mediated by the transport function of FABP3, and expectedly, overexpressing $FABP3^{F16S}$ failed to reduce taurine as compared to $FABP3^{WT}$ in H1975 cells (Fig. 5C). These results suggested that upregulation of FABP3 stimulates transport of AA to react with taurine and thus reduces global-AA in LUAD cells.

Reasoning that FABP3 works as a downstream of cir93 (Fig. 4C and Supplementary Fig. S4B-C), we wondered whether cir93 is also linked with FABP3-mediated manipulation of taurine and global-AA. Overexpressing cir93 in H1975 cells led to simultaneous reductions of taurine and global-AA, and they were entirely abolished upon knocking out FABP3 (Fig. 5D-E), demonstrating that cir93 regulates taurine and global-AA via FABP3. By contrast, inhibiting cir93 via anti-cir93 in A549 cells induced taurine and global-AA at the same time (Fig. 5F-G). Thus, manipulating taurine and global-AA is the downstream effect of cir93 in LUAD cells. In addition, co-incubation H1975 cells with plasma exosome from LUAD also resulted in lower levels of taurine and global-AA as compared to the exosome from healthy individuals (Fig. 5H-I). Due to the importance of AA in ferroptosis, exosome-desensitized LUAD cells to ferroptosis might partially via reduction of global-AA in a cir93-FABP3-taurine-dependent way.

To further verify the essential roles of taurine to reduce global-AA and desensitize LUAD cells to ferroptosis, we tried to eliminate endogenous taurine in LUAD cells. CDO1 and CSAD are critical for the synthesis of taurine (illustrated in Fig. 5J). By simultaneously knocking CDO1 and CSAD down in H1975 cells, taurine was significantly reduced and could not be further declined anymore by overexpressing cir93 or FABP3 (Fig. 5K), suggesting that sufficient taurine are prerequisites for cir93 and FABP3 to regulate taurine itself. Of note, taurine was indeed essential for cir93 and FABP3 to reduce global-AA (Fig. 5L). We then investigated whether taurine is indispensable for cir93 and FABP3 to desensitize LUAD cells to ferroptosis and reduce lipid ROS generation. Once upon taurine was depleted, erastin- and RSL3-induced ferroptosis and lipid ROS generation were significantly aggravated at basal levels; however, the restore effects by cir93 and FABP3 were all blocked (Fig. 5M and Supplementary Fig. S5D), suggesting that taurine is basically anti-ferroptotic and essential for cir93 and FABP3 to desensitize LUAD cells to ferroptosis. Via evaluating the fraction of the oxidized C11-$BODIPY^{581/591}$ and MDA concentration in the implanted LUAD in mice, the essential role of taurine for cir93 and FABP3 to reduce lipid peroxidation following administrating PKE in vivo was further verified (Fig. 5N-O and Supplementary Fig. S5E).

NAT prevented AA incorporation into the plasma membrane in LUAD cells

As described above, we used a click chemistry-based method to evaluate AA incorporation into the plasma membrane (Fig. 3F and 4G); however, click chemistry was performed when excessive exogenous alkyne-labeled AA was added. In such conditions, overexpressing cir93 and FABP3 still prevented AA

incorporation into the plasma membrane although endogenous global-AA could also be reduced by cir93 and FABP3 (Fig. 5E, 5G, 5L, 6A-B and Supplementary Fig. S6A), hinting that other mechanism might be simultaneously involved. Reasoning that AA consume is accompanied with NAT generation (illustrated in Fig. 5B); we speculated that the nascent NAT might be essential for the function of cir93 and FABP3. As expected, the relationships among cir93, FABP3 and NAT were established in H1975 cells (Fig. 6C-D). Also, taurine was essential for cir93 and FABP3 to elevate NAT in H1975 cells and implanted tumors (Fig. 6E and Supplementary Fig. S6B). Interestingly, compared to plasma exosome from healthy individuals, co-incubation of the one from LUAD led to a higher level of intracellular-NAT in H1975 cells (Fig. 6F), further indicating that elevating NAT is a critical event for exosome to desensitize LUAD cells to ferroptosis. To provide direct evidences supporting the role of NAT to prevent AA incorporation into the plasma membrane, NAT was directly incubated with H1975 cells, and such function of NAT was confirmed (Fig. 6G-H). Then, we investigated whether NAT desensitizes LUAD cells to ferroptosis, and found that erastin- and RSL3-induced induction of cell death and lipid peroxidation as well as reduction of cell viability could be mitigated in the presence of NAT (Fig. 6I-J and Supplementary Fig. S6C-E). Thus, cir93- and FABP3-desensitized LUAD cells to ferroptosis might also via stimulated generation of NAT to prevent AA incorporation into the plasma membrane.

Next, we investigated the related mechanisms. As known, ACSL4, LPCAT3 and PLTP are enzymes involved in incorporation of AA into the plasma membrane (illustrated in Fig. 6K, and Ref. 40, 41, we therefore tested whether NAT affects these enzymes, and noticed that they were all reduced by NAT dose-dependently in H1975 cells (Fig. 6L). By comparing fold changes of ACSL4, LPCAT3 and PTLP with or without co-incubation of plasma exosome, we found that 78% (78/100), 67% (67/100) and 70% (70/100) of the one from LUAD patients could reduce ACSL4, LPCAT3 and PTLP to a remaining level of less than 50%; however, similar effects were found for only 12% (12/100), 12% (12/100) and 15% (15/100) of the one from healthy individuals (Fig. 6M-N). Together, NAT-mediated downregulation of enzymes that associated with AA incorporation into the plasma membrane is equally important for exosome, cir93 and FABP3 to desensitize LUAD cells to ferroptosis.

The correlations among exosomal- and intracellular-cir93, FABP3, taurine and NAT in LUAD

To further verify the conclusions draw from above cell- and mice-based experiments (Fig. 1-6), we evaluated correlations among exosomal- and intracellular-cir93, FABP3, taurine and NAT in human LUAD specimens. Similar to intracellular-cir93 (Fig. 2B-C), FABP3 was also elevated in our LUAD cohort (n=250, Supplementary Fig. S7A). A significant correlation between FABP3 and intracellular-cir93 was revealed in LUAD (n=250, Fig. 7A). Moreover, taurine was negatively correlated with intracellular-cir93 and FABP3 (Fig. 7B-C). By contrast, positive correlations among NAT, intracellular-cir93 and FABP3 were identified in LUAD (Fig. 7D-E). To further evaluate the close relationship between exosomal- and intracellular-cir93, matched plasma and tissue specimens were obtained from same LUAD patients (n=15), and we found that exosomal-cir93 correlated well with intracellular-cir93 and FABP3 (Supplementary Fig. S7B-C). Therefore, the close relationships among exosomal- and intracellular-cir93, FABP3, taurine and NAT were established in LUAD.

Ferroptosis resistance and poor survival outcome predicted by high levels of cir93 and FABP3 in LUAD

PDX mouse models are promising tools to evaluate drug efficacy in vivo. We compared efficacy of PKE in two PDX mice models expressing distinct levels of cir93 and FABP3 (Fig. 7F), and noticed that higher levels of cir93 and FABP3 in PDX#2 resulted in less suppressions of tumor growth and lower 4-HNE levels following PKE administration as compared to PDX#1, which had relative lower levels of cir93 and FABP3 (Fig. 7F-G and Supplementary Fig. S7D), further demonstrating that cir93 and FABP3 play roles to stimulate tumor growth and desensitize cells to ferroptosis in LUAD. Via evaluating tissue slices of PDX ex vivo, we also found that PDX#2 was more resistant to erastin-induced ferroptosis in comparison to PDX#1 (Fig. 7H). Overall survival (OS) was subsequently evaluated for PDX mouse models, and PDX#2 demonstrated a shorter OS than PDX#1 (Fig. 7I). Shorter OS was also observed in those LUAD patients with higher levels of cir93 and FABP3 (n=41) compared to those with lower levels (n=41, Fig. 7J). These data demonstrated that ferroptosis resistance and poor survival in LUAD can be predicted by high levels of cir93 and FABP3.

Blocking exosome improved ferroptosis-based treatment

Reasoning that exosome from LUAD desensitizes cells to ferroptosis (Fig. 1-6); we wondered whether blocking biosynthesis of exosome could improve ferroptosis-based treatment. To this end, we further co-administrated PKE-treated A549-based CDX mice with GW4869. We found that co-treating mice with GW4869 resulted in more significant impairments of tumor growth and longer OS as compared to those treated with PKE alone (Fig. 7K-M). The aggravated elevation of MDA further confirmed that the effects were through a lipid peroxidation-dependent manner (Fig. 7N). Together, co-treating with agents that can block biosynthesis and function of exosome might be helpful to improve ferroptosis-based therapy against LUAD.

Discussion

Ferroptosis occurs when excessive lipid peroxides cannot be promptly eliminated [4, 5, 40]. To study the resistance of ferroptosis, prior studies have mainly focused on the effects of intracellular antioxidant systems; however, extracellular signaling is less concerned. Although a few studies have demonstrated that exosome exerts roles to suppress ferroptosis in miRNAs- or proteins-dependent manners [42, 43]. To the best of our knowledge, we proposed for the first time that exosome and circRNA are also capable of desensitizing LUAD cells to ferroptosis via a FABP3-dependent reduction of global-AA and prevention of AA incorporation into the plasma membrane. Such effects finally lead to a suppression of lipid peroxidation (Fig. 8). Prior studies also suggested that exosome secreted from cancer-associated fibroblasts (CAFs) and mesenchymal stem cells (MSCs) in tumor microenvironment play key roles to suppress ferroptosis [42, 44]. However, in the present study, the knowledge might be expanded because we have revealed that exosome released from tumor cells themselves has the capacity to elevate intracellular-cir93 for the function to upregulate FABP3 and desensitize LUAD cells to ferroptosis (Fig. 8).

Other than the most well accepted function to absorb miRNAs as ceRNA sponges [17], circRNAs can also directly interact with protein(s) to exercise physiological functions [34, 35]. In the present study, we have added another example indicating that the cir93-FABP3 interaction is required for the upregulation of FABP3 in LUAD cells. However, the mechanism underlying how cir93 elevates FABP3 is still unknown. Recently, circRNA cerebellar degeneration-related protein 1 transcript antisense (CDR1as) has been revealed to directly interact with p53 via the p53 DNA binding domain (DBD) domain. Interestingly, such interaction also disrupts complex formation between p53 and its Ubiquitin E3 ligase (E3) mouse double minute 2 homolog (MDM2), and finally protects p53 from degradation and increases its expression [45]. Reasoning that the cir93-FABP3 interaction is also critical for cir93 to lift FABP3 expression, cir93 might also interfere ubiquitination of FABP3. However, the genuine E3 involved is unclear and needs to be further identified and verified.

Phosphoethanolamines (PE)-containing AA is one of the key phospholipids that undergo peroxidation and essential for ferroptosis [20, 33]. Evidences demonstrate that supplementing AA sensitizes cells to ferroptosis [46]. However, the regulation of AA per se is not completely known. In this study, we elucidated that global-AA can be reduced through its reaction with taurine, and such process is boosted by FABP3. As known, FABP3 is a critical factor for PUFA transport, with no exception for AA [36, 37]. Our data supported that the reaction between AA and taurine is also indispensable from the transport function of FABP3. Reasoning that FABP3 has the ability to transport AA to proteins, such as α-Synuclein [36], we hypothesize that some certain proteins might work as adaptor platform, providing reaction site for AA and taurine. However, such proteins are still unknown and should be identified in our future study. Interestingly, the product of AA and taurine, i.e. NAT prevents AA incorporation into the plasma membrane, thus further reducing the opportunity for PUFA peroxidation in the membrane fraction. NAT reduces ACSL4, LPCAT3 and PLTP, which are all essential for AA incorporation into the plasma membrane [40, 41]. Of note, NAT activates transient receptor potential vanilloid 1 (TRPV1) channel and Ca^{2+} [47]; however, whether NAT suppresses the three enzymes via one common mechanism, such as TRPV1 and Ca^{2+}, is unclear and worth investigating in the future.

Cellular protection against oxidative damage in ferroptosis is organized by antioxidant system. Antioxidants, such as glutathione (GSH), coenzyme Q10 (CoQ10) and tetrahydrobiopterin (BH4) are critical for protecting tumor cells against ferroptosis [48]. Prior findings from our lab also approve that ferroptosis is suppressed by the sustained synthesis and utilization of GSH [4, 5, 22, 49]. However, antioxidants that protect against ferroptosis are not completely known. Due to the role of taurine to reduce global-AA and generate NAT, taurine is essential to prevent excessive lipid peroxidation, and thus can be regarded as a newly discovered antioxidant protecting against ferroptosis.

Recently, ferroptosis-based therapy has been recognized as a potential approach to treat against cancer [6, 32]. However, even the cancer-killing effect of sorafenib, a FDA-approved small molecule compound for cancer therapy, has been linked to ferroptosis [50], and other ferroptosis-related gene therapies, as well as nanomaterials are in development [51], it is still a long way for ferroptosis-based therapy to be applied in clinical because of its off-target effects, unsatisfactory efficacy, unguaranteed safety and low in vivo

stability of the inducers [6, 32, 52]. Here, we provide several new ferroptosis targets including cir93, FABP3, taurine and NAT, and their functions all link with exosome. Indeed, the efficacy of ferroptosis can be synergized by blocking exosome biosynthesis in our in vivo preclinical models, thus providing new strategy to improve ferroptosis-based therapy.

Conclusions

In conclusion, the roles of exosome and cir93 are critical to desensitize LUAD to ferroptosis. Blocking exosome will be helpful to enhance efficacy of ferroptosis-based therapy in future treatment against LUAD.

Abbreviations

4-HNE, anti-4-hydroxynonenal; AA, arachidonic acid; AAV5, adeno-associated virus 5; ACSL4, acyl-CoA synthetase long-chain family member; AdA, adrenal acid; ALIX, ALG-2 interacting protein X; ALK, anaplastic lymphoma kinase; BH4, tetrahydrobiopterin; BME, basement membrane extract; CAFs, cancer-associated fibroblasts; CD63, cluster of differentiation 63; CD9, cluster of differentiation 9; CDO1, cysteine dioxygenase type 1; CDR1as, circRNA cerebellar degeneration-related protein 1 transcript antisense; CDX, cell-derived xenograft; ceRNAs, competing endogenous RNAs ; cir34, circRNA_100934; cir93, circRNA_101093; circRNA, circular RNA; CoQ10, coenzyme Q10; CSAD, cysteine sulfinic acid decarboxylase; DBD, DNA binding domain; DFO, deferoxamine; DIG, digoxigenin; DMA, 5,5-(N-N-dimethyl)-amiloride hydrochloride; DMEM, Dulbecco's modified eagle medium; DMSO, dimethyl sulfoxide; DPBS, Dulbecco's phosphate buffered saline; EGFR, epidermal growth factor receptor; ELISA, enzyme linked immunosorbent assay; EpCAM, epithelial cell adhesion molecule; ER, endoplasmic reticulum; ESI, electrospray ionization; F, phenylalanine; FABP3, fatty acid-binding protein 3; FABPs, fatty acid-binding proteins; FBS, fetal bovine serum; Fer-1, Ferrostatin-1; FISH, fluorescence in situ hybridization; GSH, glutathione; HIC1, hypermethylated in cancer 1; HNF4a, hepatocyte nuclear factor alpha; HPLC, high performance liquid chromatograph; IB, immunoblotting; IF, immunofluorescence; IHC, immunohistochemistry; kRAS, v-Ki-ras2 Kirsten rat sarcoma viral oncogene homolog; LPCAT3, lysophosphatidylcholine acyltransferase 3; LUAD, lung adenocarcinoma; m^6A, N^6-methyladenosine; MDA, malondialdehyde; MDM2, mouse double minute 2 homolog; MS, mass spectrometry; MSCs, mesenchymal stem cells; NAT, N-arachidonoyl taurine; NUP107, nucleoporin 107; ORF, open reading frame; OS, overall survival; p53, tumor protein 53; PAR-CLIP, photoactivatable ribonucleoside-enhanced crosslinking and immunoprecipitation; PDX, patient-derived xenograft; PE, phosphoethanolamines; PFA, paraformaldehyde; PI, propidium iodide; PKE, piperazine erastin; PLTP, phospholipid transfer protein; PUFA, poly-unsaturated fatty acids; qPCR, quantitative RT-PCR; RIP, RNA, immunoprecipitation; ROS, reactive oxygen species; RSL3, ras-selective lethal small molecule 3; S, serine; SSC, saline sodium citrate; TEM, transmission electron microscope; TRPV1, transient receptor potential vanilloid 1; TSG101, tumor susceptibility 101; αSMA, alpha smooth muscle actin.

Declarations

Ethics approval and consent to participate

All the informed written consents were obtained. The study including those for animals were approved by the institutional ethics committee of Shanghai Chest Hospital.

Consent for publication

Not applicable.

Availability of data and materials

The datasets generated and/or analysed during the current study are available in the ProteomeXchange Consortium under the accession number PXD025491 (username: reviewer_pxd025491@ebi.ac.uk, and the password: U8S9cjhj) and PXD025575 (username: reviewer_pxd025575@ebi.ac.uk, and the password: 9h0oFtLK).

Competing interests

None.

Funding

This work was supported by the National Natural Science Foundation of China (81871907, 81822029, 81872288, 81902315, 81902869, 81774291), Shanghai Municipal Education Commission—Gaofeng Clinical Medicine (20191834), Project of Clinical Research Supporting System, Clinical Medicine First-class Discipline, Grant Support “Chen Guang” project supported by Shanghai Municipal Education Commission and Shanghai Education Development Foundation (18CG16), Shanghai Sailing Program (19YF1444800), Science and technology commission of Shanghai municipality project (19140902600, 21140902800), and Nurture projects for basic research of Shanghai Chest Hospital (2018YNJCM01, 2019YNJCM06).

Author’s Contributions

X. Z. researched, analyzed data and wrote the manuscript. Y. X. collected and analyzed clinical samples, and researched data. L. M. researched and analyzed data. K. Y. collected and analyzed clinical samples, and researched data. Y. N. designed and organized the pictures. X. X. researched and analyzed data. Y. S. performed bioinformatics analysis. S. G., X. X., Y. W., S. Q., J. C. and H. W. researched and analyzed data, and contributed to the discussion. X. T. constructed the plasmids. Y. M. performed the mouse experiments. F. M. researched and analyzed data. Y. Q. and Y. Y. designed the study. J. W. designed the study and wrote the manuscript.

Acknowledgements

None.

References

1. Herbst RS, Morgensztern D, Boshoff C. The biology and management of non-small cell lung cancer. Nature. 2018;553(7689):446–54.
2. Skoulidis F, Heymach JV. Co-occurring genomic alterations in non-small-cell lung cancer biology and therapy. Nat Rev Cancer. 2019;19(9):495–509.
3. Leonetti A, Sharma S, Minari R, Perego P, Giovannetti E, Tiseo M. Resistance mechanisms to osimertinib in EGFR-mutated non-small cell lung cancer. Br J Cancer. 2019;121(9):725–37.
4. Ma L, Chen T, Zhang X, Miao Y, Tian X, Yu K, Xu X, Niu Y, Guo S, Zhang C, et al. The m(6)A reader YTHDC2 inhibits lung adenocarcinoma tumorigenesis by suppressing SLC7A11-dependent antioxidant function. Redox Biol. 2021;38:101801.
5. Ma L, Zhang X, Yu K, Xu X, Chen T, Shi Y, Wang Y, Qiu S, Guo S, Cui J, et al. Targeting SLC3A2 subunit of system XC(-) is essential for m(6)A reader YTHDC2 to be an endogenous ferroptosis inducer in lung adenocarcinoma. Free Radic Biol Med. 2021;168:25–43.
6. Hassannia B, Vandenabeele P, Vanden Berghe T. Targeting Ferroptosis to Iron Out Cancer. Cancer Cell. 2019;35(6):830–49.
7. Alvarez SW, Sviderskiy VO, Terzi EM, Papagiannakopoulos T, Moreira AL, Adams S, Sabatini DM, Birsoy K, Possemato R. NFS1 undergoes positive selection in lung tumours and protects cells from ferroptosis. Nature. 2017;551(7682):639–43.
8. Anderstam B, Vaca C, Harms-Ringdahl M. Lipid peroxide levels in a murine adenocarcinoma exposed to hyperthermia: the role of glutathione depletion. Radiat Res. 1992;132(3):296–300.
9. Kamerkar S, LeBleu VS, Sugimoto H, Yang S, Ruivo CF, Melo SA, Lee JJ, Kalluri R. Exosomes facilitate therapeutic targeting of oncogenic KRAS in pancreatic cancer. Nature. 2017;546(7659):498–503.
10. Sung BH, von Lersner A, Guerrero J, Krystofiak ES, Inman D, Pelletier R, Zijlstra A, Ponik SM, Weaver AM. A live cell reporter of exosome secretion and uptake reveals pathfinding behavior of migrating cells. Nat Commun. 2020;11(1):2092.
11. Mathieu M, Martin-Jaular L, Lavieu G, Thery C. Specificities of secretion and uptake of exosomes and other extracellular vesicles for cell-to-cell communication. Nat Cell Biol. 2019;21(1):9–17.
12. Brown CW, Amante JJ, Chhoy P, Elaimy AL, Liu H, Zhu LJ, Baer CE, Dixon SJ, Mercurio AM. Prominin2 Drives Ferroptosis Resistance by Stimulating Iron Export. Dev Cell. 2019;51(5):575–86 e574.
13. Shang A, Gu C, Wang W, Wang X, Sun J, Zeng B, Chen C, Chang W, Ping Y, Ji P, et al. Exosomal circPACRGL promotes progression of colorectal cancer via the miR-142-3p/miR-506-3p- TGF-beta1 axis. Mol Cancer. 2020;19(1):117.
14. Qiu M, Xia W, Chen R, Wang S, Xu Y, Ma Z, Xu W, Zhang E, Wang J, Fang T, et al. The Circular RNA circPRKCI Promotes Tumor Growth in Lung Adenocarcinoma. Cancer Res. 2018;78(11):2839–51.

15. Long F, Lin Z, Li L, Ma M, Lu Z, Jing L, Li X, Lin C. Comprehensive landscape and future perspectives of circular RNAs in colorectal cancer. Mol Cancer. 2021;20(1):26.
16. Wang Y, Liu J, Ma J, Sun T, Zhou Q, Wang W, Wang G, Wu P, Wang H, Jiang L, et al. Exosomal circRNAs: biogenesis, effect and application in human diseases. Mol Cancer. 2019;18(1):116.
17. Zhong Y, Du Y, Yang X, Mo Y, Fan C, Xiong F, Ren D, Ye X, Li C, Wang Y, et al. Circular RNAs function as ceRNAs to regulate and control human cancer progression. Mol Cancer. 2018;17(1):79.
18. Friedmann Angeli JP, Krysko DV, Conrad M. Ferroptosis at the crossroads of cancer-acquired drug resistance and immune evasion. Nat Rev Cancer. 2019;19(7):405–14.
19. Yamashima T. 'PUFA-GPR40-CREB signaling' hypothesis for the adult primate neurogenesis. Prog Lipid Res. 2012;51(3):221–31.
20. Kagan VE, Mao G, Qu F, Angeli JP, Doll S, Croix CS, Dar HH, Liu B, Tyurin VA, Ritov VB, et al. Oxidized arachidonic and adrenic PEs navigate cells to ferroptosis. Nat Chem Biol. 2017;13(1):81–90.
21. Zhang X, Yu K, Ma L, Qian Z, Tian X, Miao Y, Niu Y, Xu X, Guo S, Yang Y, et al. Endogenous glutamate determines ferroptosis sensitivity via ADCY10-dependent YAP suppression in lung adenocarcinoma. Theranostics. 2021;11(12):5650–74.
22. Zhang X, Du L, Qiao Y, Zhang X, Zheng W, Wu Q, Chen Y, Zhu G, Liu Y, Bian Z, et al. Ferroptosis is governed by differential regulation of transcription in liver cancer. Redox Biol. 2019;24:101211.
23. Xie Y, Dang W, Zhang S, Yue W, Yang L, Zhai X, Yan Q, Lu J. The role of exosomal noncoding RNAs in cancer. Mol Cancer. 2019;18(1):37.
24. Zhou B, Xu K, Zheng X, Chen T, Wang J, Song Y, Shao Y, Zheng S. Application of exosomes as liquid biopsy in clinical diagnosis. Signal Transduct Target Ther. 2020;5(1):144.
25. Fanale D, Taverna S, Russo A, Bazan V. Circular RNA in Exosomes. Adv Exp Med Biol. 2018;1087:109–17.
26. Zhang X, Wang S, Wang H, Cao J, Huang X, Chen Z, Xu P, Sun G, Xu J, Lv J, et al. Circular RNA circNRIP1 acts as a microRNA-149-5p sponge to promote gastric cancer progression via the AKT1/mTOR pathway. Mol Cancer. 2019;18(1):20.
27. Zhu X, Wang X, Wei S, Chen Y, Chen Y, Fan X, Han S, Wu G. hsa_circ_0013958: a circular RNA and potential novel biomarker for lung adenocarcinoma. FEBS J. 2017;284(14):2170–82.
28. Li Y, Zheng Q, Bao C, Li S, Guo W, Zhao J, Chen D, Gu J, He X, Huang S. Circular RNA is enriched and stable in exosomes: a promising biomarker for cancer diagnosis. Cell Res. 2015;25(8):981–4.
29. Bremnes RM, Donnem T, Al-Saad S, Al-Shibli K, Andersen S, Sirera R, Camps C, Marinez I, Busund LT. The role of tumor stroma in cancer progression and prognosis: emphasis on carcinoma-associated fibroblasts and non-small cell lung cancer. J Thorac Oncol. 2011;6(1):209–17.
30. Thomas D, Radhakrishnan P. Tumor-stromal crosstalk in pancreatic cancer and tissue fibrosis. Mol Cancer. 2019;18(1):14.
31. Xie Y, Hou W, Song X, Yu Y, Huang J, Sun X, Kang R, Tang D. Ferroptosis: process and function. Cell Death Differ. 2016;23(3):369–79.

32. Chen X, Kang R, Kroemer G, Tang D. **Broadening horizons: the role of ferroptosis in cancer**. *Nat Rev Clin Oncol* 2021.
33. Magtanong L, Ko PJ, To M, Cao JY, Forcina GC, Tarangelo A, Ward CC, Cho K, Patti GJ, Nomura DK, et al. Exogenous Monounsaturated Fatty Acids Promote a Ferroptosis-Resistant Cell State. Cell Chem Biol. 2019;26(3):420–32 e429.
34. Zhou WY, Cai ZR, Liu J, Wang DS, Ju HQ, Xu RH. Circular RNA: metabolism, functions and interactions with proteins. Mol Cancer. 2020;19(1):172.
35. Huang A, Zheng H, Wu Z, Chen M, Huang Y. Circular RNA-protein interactions: functions, mechanisms, and identification. Theranostics. 2020;10(8):3503–17.
36. Cheng A, Shinoda Y, Yamamoto T, Miyachi H, Fukunaga K. Development of FABP3 ligands that inhibit arachidonic acid-induced alpha-synuclein oligomerization. Brain Res. 2019;1707:190–7.
37. Shioda N, Yabuki Y, Kobayashi Y, Onozato M, Owada Y, Fukunaga K. FABP3 protein promotes alpha-synuclein oligomerization associated with 1-methyl-1,2,3,6-tetrahydropiridine-induced neurotoxicity. J Biol Chem. 2014;289(27):18957–65.
38. Liin SI, Larsson JE, Barro-Soria R, Bentzen BH, Larsson HP. **Fatty acid analogue N-arachidonoyl taurine restores function of IKs channels with diverse long QT mutations**. *Elife* 2016, 5.
39. Kumar A, Misra BB. Challenges and Opportunities in Cancer Metabolomics. Proteomics. 2019;19(21–22):e1900042.
40. Stockwell BR, Friedmann Angeli JP, Bayir H, Bush AI, Conrad M, Dixon SJ, Fulda S, Gascon S, Hatzios SK, Kagan VE, et al. Ferroptosis: A Regulated Cell Death Nexus Linking Metabolism, Redox Biology, and Disease. Cell. 2017;171(2):273–85.
41. Jalil A, Bourgeois T, Menegaut L, Lagrost L, Thomas C, Masson D. **Revisiting the Role of LXRs in PUFA Metabolism and Phospholipid Homeostasis**. *Int J Mol Sci* 2019, 20(15).
42. Zhang H, Deng T, Liu R, Ning T, Yang H, Liu D, Zhang Q, Lin D, Ge S, Bai M, et al. CAF secreted miR-522 suppresses ferroptosis and promotes acquired chemo-resistance in gastric cancer. Mol Cancer. 2020;19(1):43.
43. Song Z, Jia G, Ma P, Cang S. Exosomal miR-4443 promotes cisplatin resistance in non-small cell lung carcinoma by regulating FSP1 m6A modification-mediated ferroptosis. Life Sci. 2021;276:119399.
44. Song Y, Wang B, Zhu X, Hu J, Sun J, Xuan J, Ge Z. Human umbilical cord blood-derived MSCs exosome attenuate myocardial injury by inhibiting ferroptosis in acute myocardial infarction mice. Cell Biol Toxicol. 2021;37(1):51–64.
45. Lou J, Hao Y, Lin K, Lyu Y, Chen M, Wang H, Zou D, Jiang X, Wang R, Jin D, et al. Circular RNA CDR1as disrupts the p53/MDM2 complex to inhibit Gliomagenesis. Mol Cancer. 2020;19(1):138.
46. Yang WS, Kim KJ, Gaschler MM, Patel M, Shchepinov MS, Stockwell BR. Peroxidation of polyunsaturated fatty acids by lipoxygenases drives ferroptosis. Proc Natl Acad Sci U S A. 2016;113(34):E4966–75.

47. Zhang M, Ruwe D, Saffari R, Kravchenko M, Zhang W. Effects of TRPV1 Activation by Capsaicin and Endogenous N-Arachidonoyl Taurine on Synaptic Transmission in the Prefrontal Cortex. Front Neurosci. 2020;14:91.
48. Kuang F, Liu J, Tang D, Kang R. Oxidative Damage and Antioxidant Defense in Ferroptosis. Front Cell Dev Biol. 2020;8:586578.
49. Guo S, Chen Y, Yang Y, Zhang X, Ma L, Xue X, Qiao Y, Wang J. TRIB2 modulates proteasome function to reduce ubiquitin stability and protect liver cancer cells against oxidative stress. Cell Death Dis. 2021;12(1):42.
50. Sun X, Ou Z, Chen R, Niu X, Chen D, Kang R, Tang D. Activation of the p62-Keap1-NRF2 pathway protects against ferroptosis in hepatocellular carcinoma cells. Hepatology. 2016;63(1):173–84.
51. Liang C, Zhang X, Yang M, Dong X. Recent Progress in Ferroptosis Inducers for Cancer Therapy. Adv Mater. 2019;31(51):e1904197.
52. Shen Z, Song J, Yung BC, Zhou Z, Wu A, Chen X. Emerging Strategies of Cancer Therapy Based on Ferroptosis. Adv Mater. 2018;30(12):e1704007.

Figures

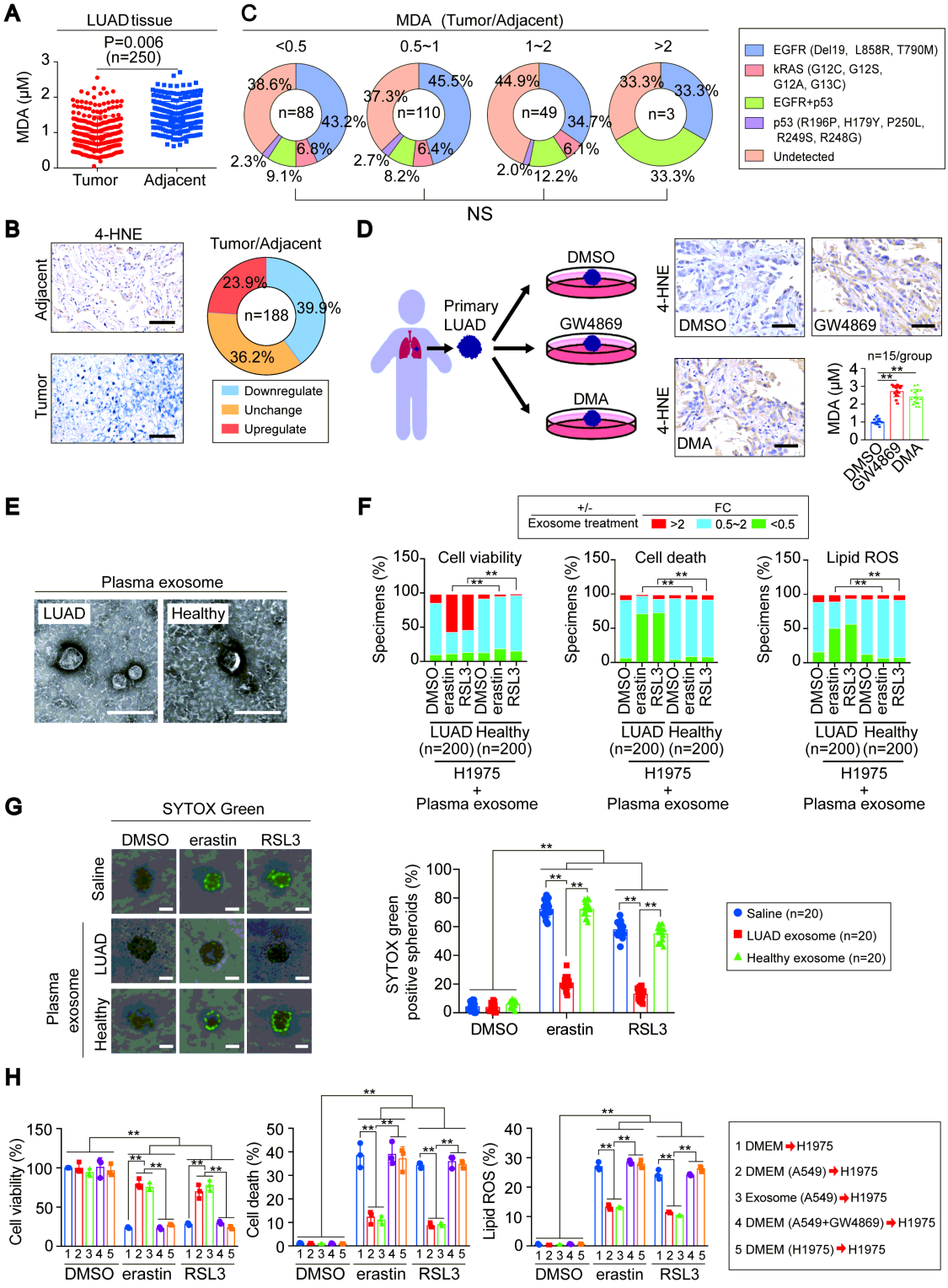

Figure 1

Exosome reduced lipid peroxidation and desensitized ferroptosis in LUAD. (A) The concentration of MDA in tumor and matched adjacent tissues of LUAD (n=250). (B) Representative IHC images for 4-HNE and the percentage of LUAD (n=188) with different 4-HNE tumor/adjacent alterations. (C) Incidence of indicated mutations in different groups of LUAD with varied MDA tumor/adjacent ratios. (D) 4-HNE was evaluated by IHC in ex vivo primary LUAD treated with DMSO, GW4869 (10 μM), or DMA (50 nM). Scale

bar, 200 μm. Also, MDA was parallel tested. (E) Representative TEM images of plasma exosome in LUAD patients and healthy individuals. Scale bar, 300 nm. (F) Percentage of exosome from LUAD patients or healthy individuals on the alterations of cell viability, cell death and lipid ROS generation, as indicated, in H1975 cells following treating with DMSO, erastin (10 μM, 16-24h), or RSL3 (5 μM, 16-24h). (G) 3D spheroids were generated by H1975 cells, which were pre-co-incubated with saline, plasma exosome from LUAD patients or healthy individuals. After formation of 3D spheroids, cell death was measured by staining with SYTOX green following treating with DMSO, erastin (10 μM, 24h), or RSL3 (5 μM, 24h). Representative images and graphed data are shown, Scale bar, 50 μm. (H) Exosome desensitized H1975 cells to ferroptosis. H1975 cells were pre-co-incubated with indicated DMEM or exosome prior to the treatment of DMSO, erastin (10 μM, 16-24h), or RSL3 (5 μM, 16-24h). Afterwards, cell viability, cell death and lipid ROS generations were measured. The data are shown as the mean ± SD from three biological replicates. **P < 0.01 indicates statistical significance. NS, non-significance. Data in A were analyzed using a student's t test. Data in C, F were analyzed using $\chi 2$ tests. Data in D were analyzed using a one-way ANOVA test. Data in G, H were analyzed using two-way ANOVA tests.

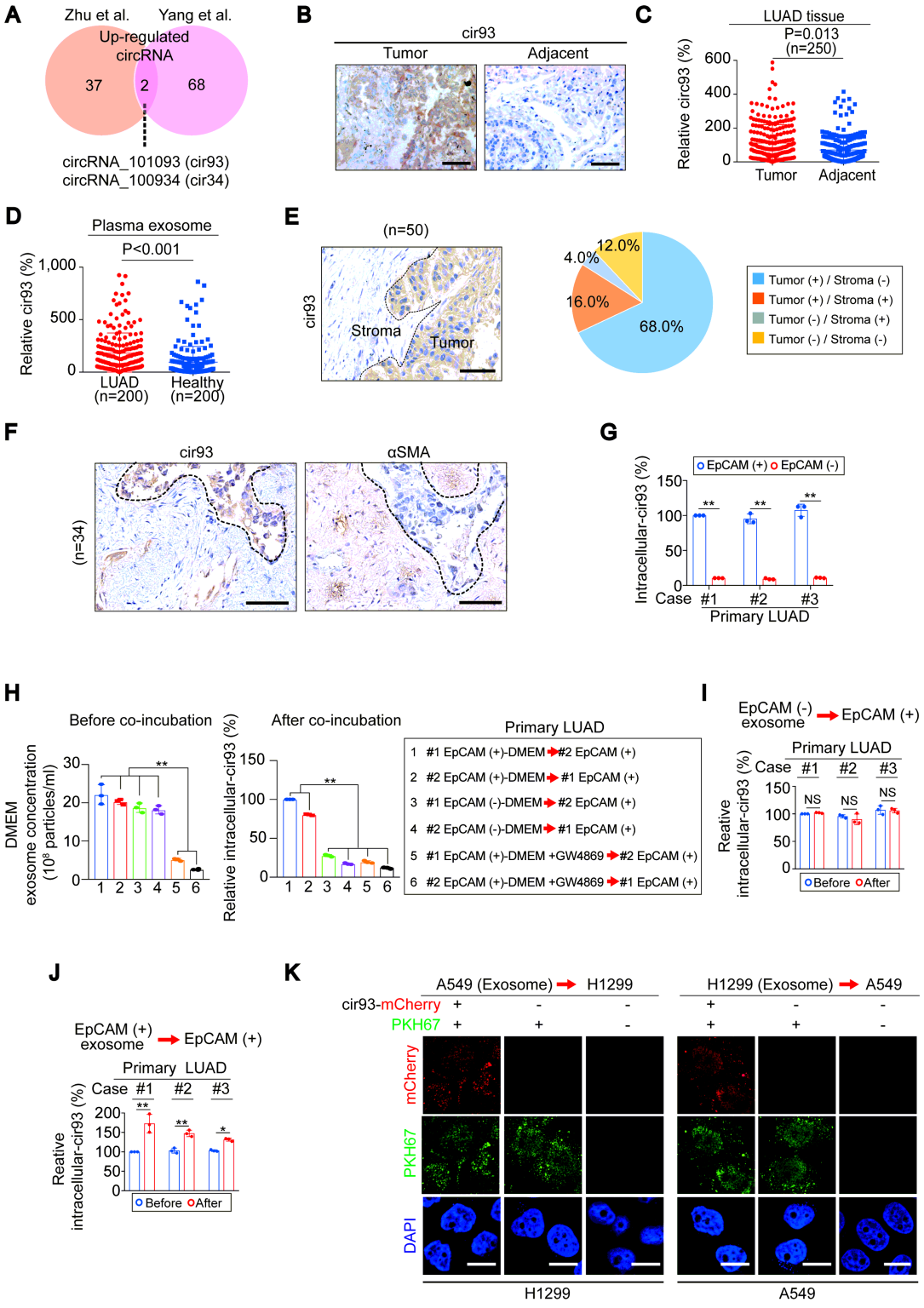

Figure 2

Exosome secreted from tumor cells themselves was essential to elevate intracellular-cir93 in LUAD. (A) CircRNA screening identified cir93 and cir34 as upregulated circRNAs in LUAD. (B-C) Images of cir93 in tumor and matched adjacent tissues of LUAD. Scale bar, 200 μm (B). The levels of cir93 were also measured by qPCR and graphed (C). (D) Exosomal-cir93 was measured by qPCR in LUAD patients (n=200) and healthy individuals (n=200). (E) Cir93 was exclusively expressed in the tumor part of LUAD.

Representative FISH image of cir93 in LUAD (n=50) is shown in the left panel, and the percentages for different cir93 expression pattern are illustrated in the right panel. Scale bar, 100 μm (F) Representative FISH and IHC images for cir93 and αSMA in the same areas of LUAD from same patients (n=34). Scale bar, 200 μm. (G) Intracellular-cir93 in EpCAM (+) and EpCAM (-) cells from 3 distinct primary LUAD, as measured by qPCR. (H) Concentrations of exosome in the indicated DMEM before co-incubation with indicated cells. Meanwhile, the levels of intracellular-cir93 in indicated cells after co-incubation with the indicated DMEM were graphed. (I-J) Intracellular-cir93 in EpCAM (+) cells before and after co-incubation of exosome from EpCAM (-) (I) and EpCAM (+) cells (J) from primary LUAD of 3 distinct patients. (K) Transmission of cir93 between A549 and H1299 cells via exosome. The exosome from A549 or H1299 cells expressing cir93-mCherry (red) was marked by PKH67 (green) and incubated with H1299 or A549 cells. Afterwards, IF was performed for the detection of cir93 and exosome. Scale bar, 20 μm. The data are shown as the mean ± SD from three biological replicates. *P < 0.05, **P < 0.01 indicates statistical significance. NS, non-significance. Data in C, D, G, I and J were analyzed using student's t tests. Data in H were analyzed using a one-way ANOVA test.

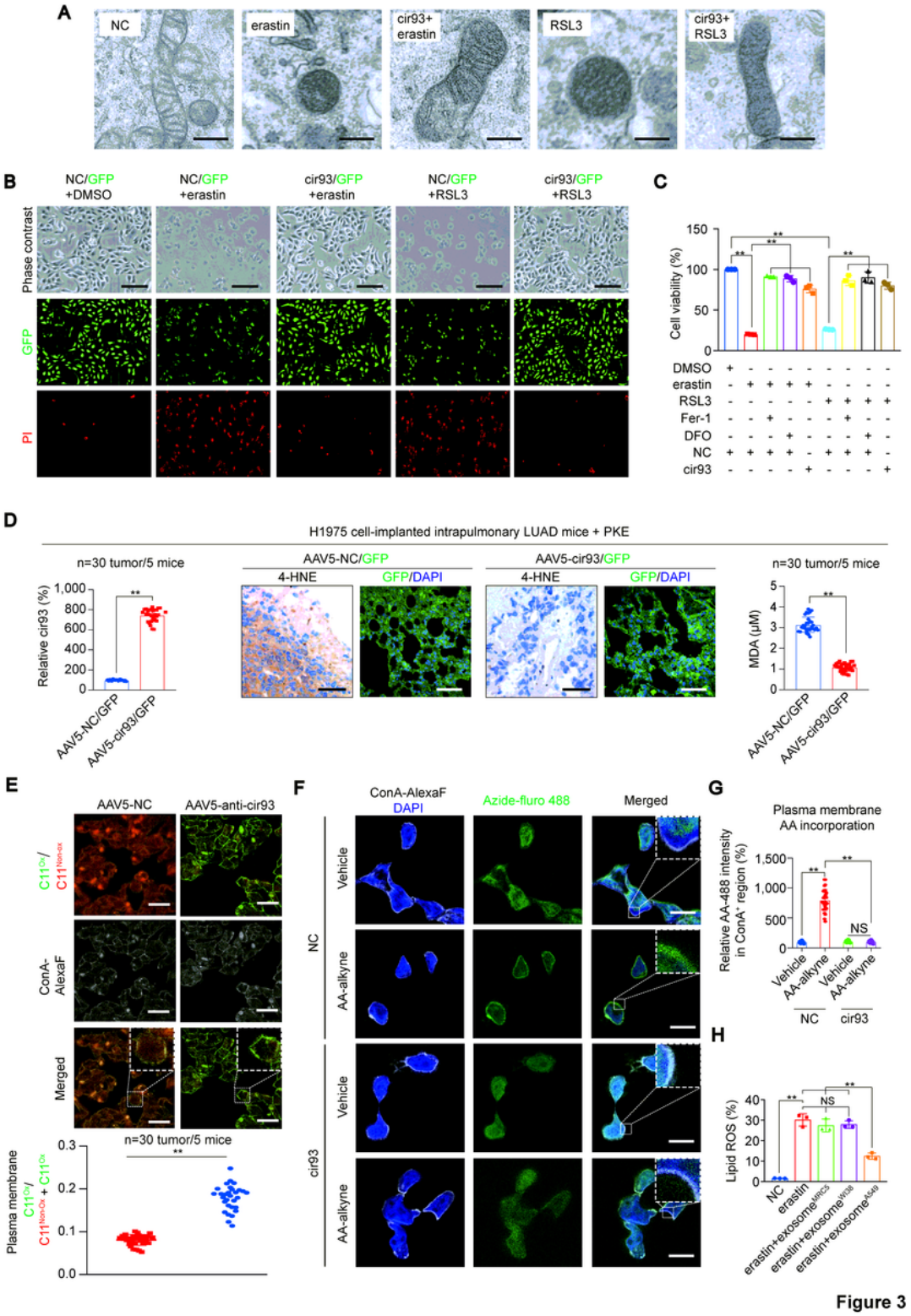

Figure 3

Figure 3

The roles of cir93 to reduce lipid peroxidation and desensitize LUAD cells to ferroptosis. (A) TEM images showing changes of mitochondria following treating with or without erastin (10 μM, 12h) or RSL3 (5 μM, 12h) in H1975 cells pre-overexpressed with or without cir93. Scale bar, 500 nm. (B) Cell death was measured by PI staining of H1975 cells co-expressing GFP with or without cir93 followed by treating with DMSO, erastin (10 μM, 12h) or RSL3 (5 μM, 12h). Scale bar, 200 μm. (C) Cell viability was measured in

H1975 cells expressing with or without cir93 following treating with DMSO, erastin (10 μM, 24h), RSL3 (5 μM, 24h), Fer-1 (1 μM, 24h), or DFO (80 μM, 24h). (D) Intracellular-cir93, 4-HNE and MDA were measured in the tumors (n=30 tumors from 5 mice/group) from H1975 cell-implanted intrapulmonary LUAD mice that intranasal pre-infected with GFP-expressing AAV5 with or without co-expressing cir93 followed by administrating mice with PKE (20mg/kg, 2 weeks). Scale bar, 200 μm. (E) Lipid peroxidation was probed by C11-BODIPY581/591 in A549 cell-implanted intrapulmonary LUAD mice intranasal infected with control AAV5 and AAV5 carrying anti-cir93. The fractions of oxidized C11-BODIPY581/591 were calculated in each group (n=30 tumors from 5 mice/group). Scale bar, 100 μm. (F-G) AA incorporation into the plasma membrane, as measured by a click chemistry-based method in H1975 cells with or without overexpression of cir93. The representative images (F) and graphed data (G) are shown. Scale bar, 50 μm. (H) Lipid ROS generation in H1975 cells pre-co-incubated with exosome, as indicated, followed by treating with or without erastin (10 μM, 16h). The data are shown as the mean ± SD from three biological replicates. **P < 0.01 indicates statistical significance. NS, non-significance. Data in C, G, H were analyzed using one-way ANOVA tests. Data in D, E were analyzed using student's t tests.

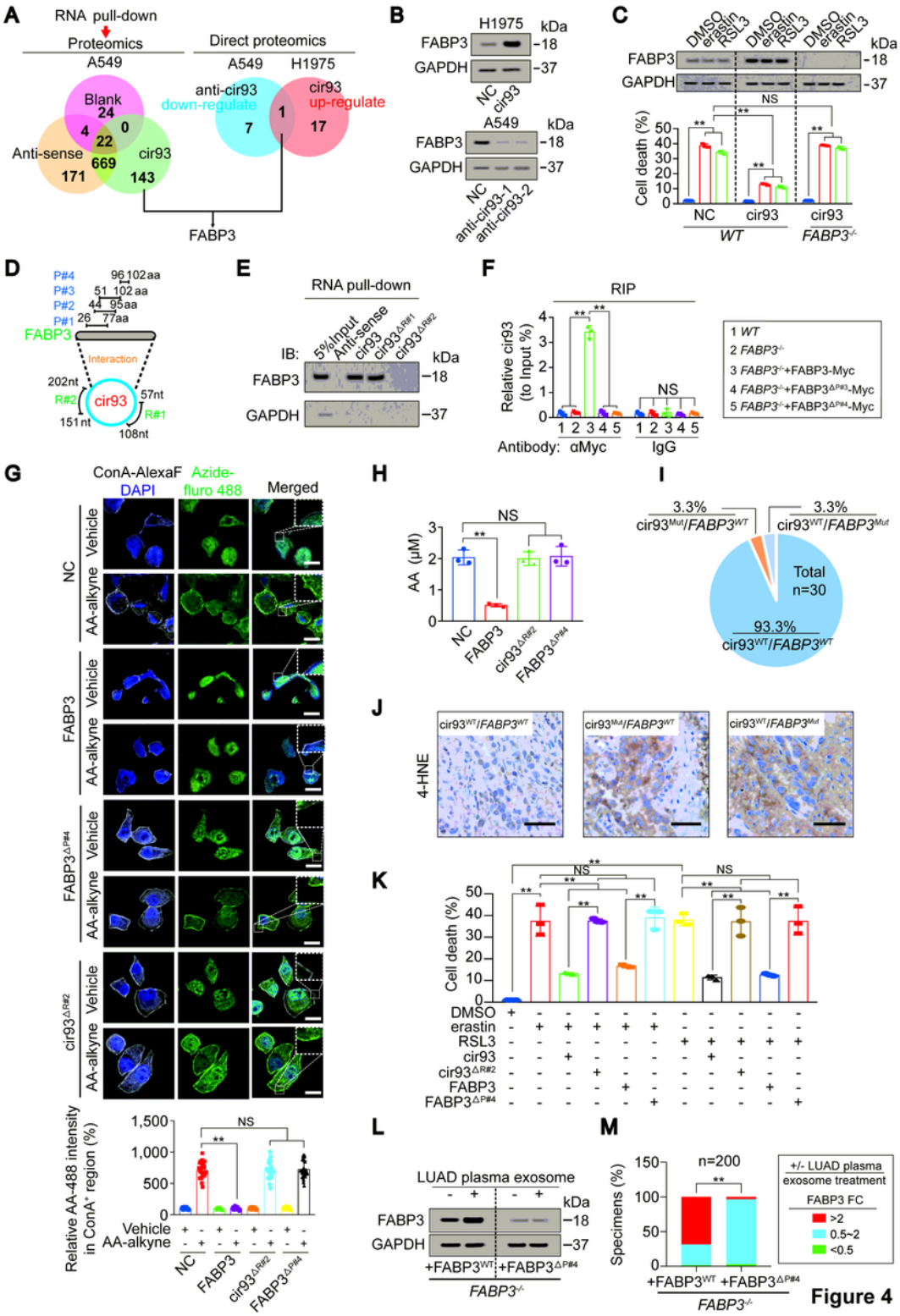

Figure 4

The cir93-FABP3 interaction was essential for reducing lipid peroxidation and desensitizing ferroptosis. (A) Venn diagram showing that FABP3 was the only protein that could be simultaneously upregulated by and interacted with cir93, as identified via RNA pull-down followed by proteomics in A549 cells and direct proteomics in both A549 and H1975 cells. The proteins that regulated by cir93 were defined as fold changes>1.5 following treatments and with a P value<0.05. (B) Representative IB images of FABP3 in

H1975 cells with or without cir93 overexpression, and in A549 cells with or without treatment of anti-cir93. (C) FABP3 expression and cell death in WT and FABP3-/- H1975 cells with or without overexpressing cir93 prior to the treatment of DMSO, erastin (10 μM, 24h) or RSL3 (5 μM, 24h). (D) Prediction of the cir93-FABP3 interactions, as revealed by catRAPID database (http://service.tartaglialab.com/page/catrapid_group). (E) RNA pull-down experiments in H1975 cells expressing WT or mutant cir93 using WT or mutant cir93 probes, as indicated, and the interaction of FABP3 was revealed by IB. (F) RIP experiments performing by anti-Myc and IgG antibodies in WT and FABP3-/- H1975 cells reconstituting with indicated Myc-tagged FABP3. (G) Click chemistry experiments demonstrating changes of AA incorporation in control cells and H1975 cells overexpressing FABP3, FABP3ΔP#4 or cir93ΔR#2. Scale bar, 50 μm. (H) Changes of global-AA in control cells and H1975 cells with indicated treatment. (I) Percentages of cir93 and FABP3 mutations in LUAD (n=30). (J) 4-HNE levels in LUAD tissue with or without cir93 and FABP3 mutations, as indicated. Scale bar, 200 μm. (K) The R#2 of cir93 and P#4 of FABP3 were essential for cir93 and FABP3 to reduce erastin- and RSL3-induced cell death in H1975 cells. Cell death was measured in H1975 cells pre-overexpressing WT, mutant cir93 or FABP3 followed by treating with DMSO, erastin (10 μM, 24h) or RSL3 (5 μM, 24h). (L-M) Representative IB images for FABP3 following co-incubation with or without LUAD plasma exosome in FABP3-/- H1975 cells reconstituting with FABP3WT or FABP3ΔP#4 (L). The incidences for plasma exosome with capacity to alter FABP3 with different fold changes (FC) are shown in panel M. The data are shown as the mean ± SD from three biological replicates (including IB). **P < 0.01 indicates statistical significance. NS, non-significance. Data in C, F, G, H, K were analyzed using one-way ANOVA tests. Data in M were analyzed using a $\chi 2$ test.

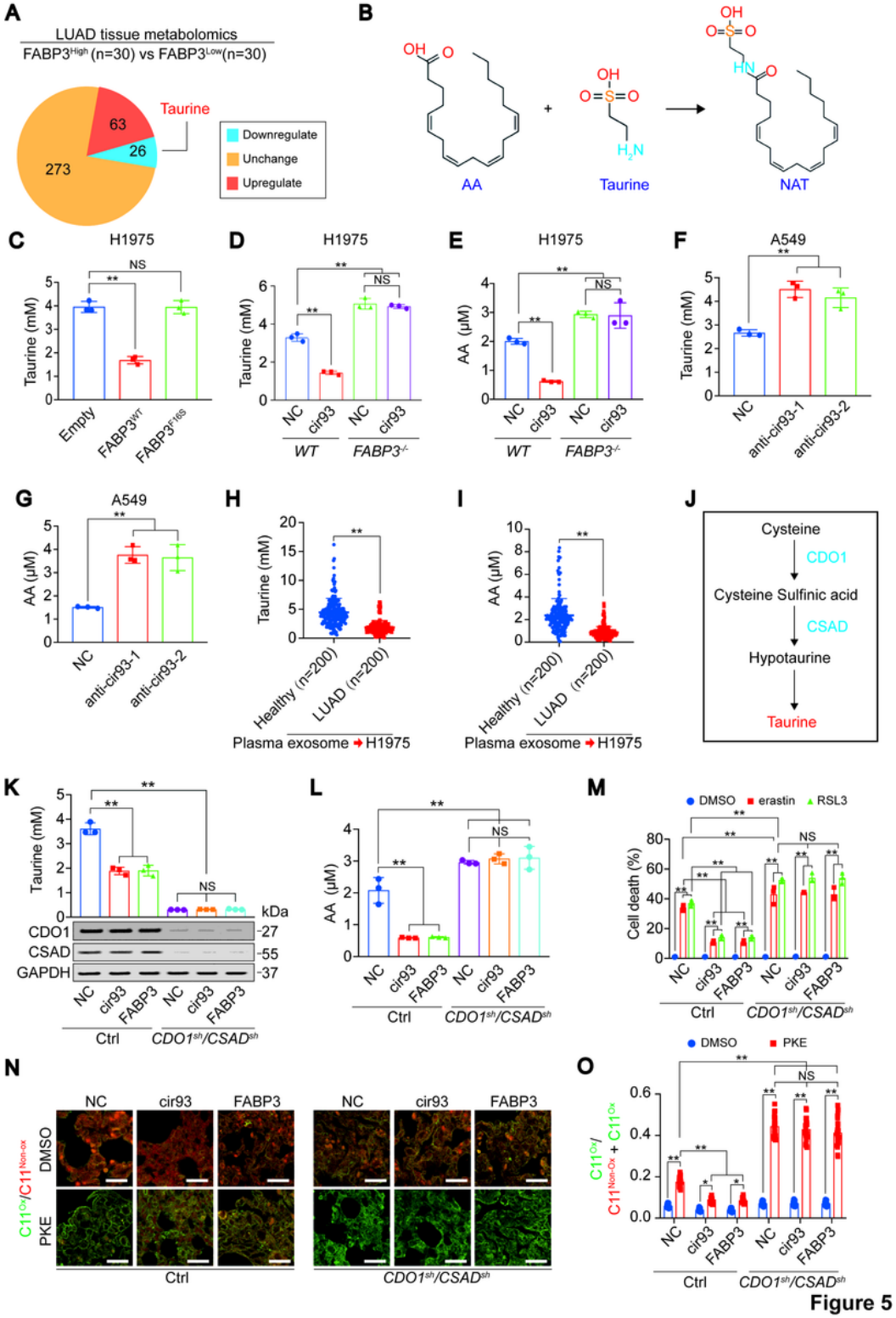

Figure 5

Figure 5

Taurine was required for cir93 and FABP3 to modulate AA. (A) Metabolomics showing the amounts of metabolites that changed among LUAD tissues expressing low (n=30) and high (n=30) levels of FABP3. (B) Schematic representation of the reaction between AA and taurine to generate NAT. (C) Reduction of taurine by FABP3 was relied on its transport function. Taurine was measured in control cells and H1975 cells overexpressing FABP3WT or FABP3F16S. (D-E) Taurine (D) and global-AA (E) was measured in WT

and FABP3-/- H1975 cells with or without overexpressing cir93. (F-G) Taurine (F) and global-AA (G) in A459 cells with or without treating with indicated anti-cir93. (H-I) Taurine (H) and global-AA (I) in H1975 cells following co-incubation of plasma exosome from healthy individuals (n=200) or LUAD patients (n=200). (J) Schematic representation of the biosynthesis of taurine. (K-M) Taurine (K), global-AA (L) and cell death (M) were measured in control cells and H1975 cells infected with shRNAs against CDO1 and CSAD followed by overexpressing with or without cir93 or FABP3. (N-O) CDXs were generated from control and H1975 cells infected with shRNAs targeting against CDO1 and CSAD followed by overexpressing with or without cir93 or FABP3. Mice were administrated with DMSO or PKE (20mg/kg, 2 weeks) before lipid peroxidation was probed by C11-BODIPY581/591. The representative images are shown in panel N, and the data were graphed in panel O. Scale bar, 200 μm. The data are shown as the mean ± SD from three biological replicates (including IB). *P < 0.05, **P < 0.01 indicates statistical significance. NS, non-significance. Data in C-G, K-M, O were analyzed using one-way ANOVA tests. Data in H, I were analyzed using student’s t tests.

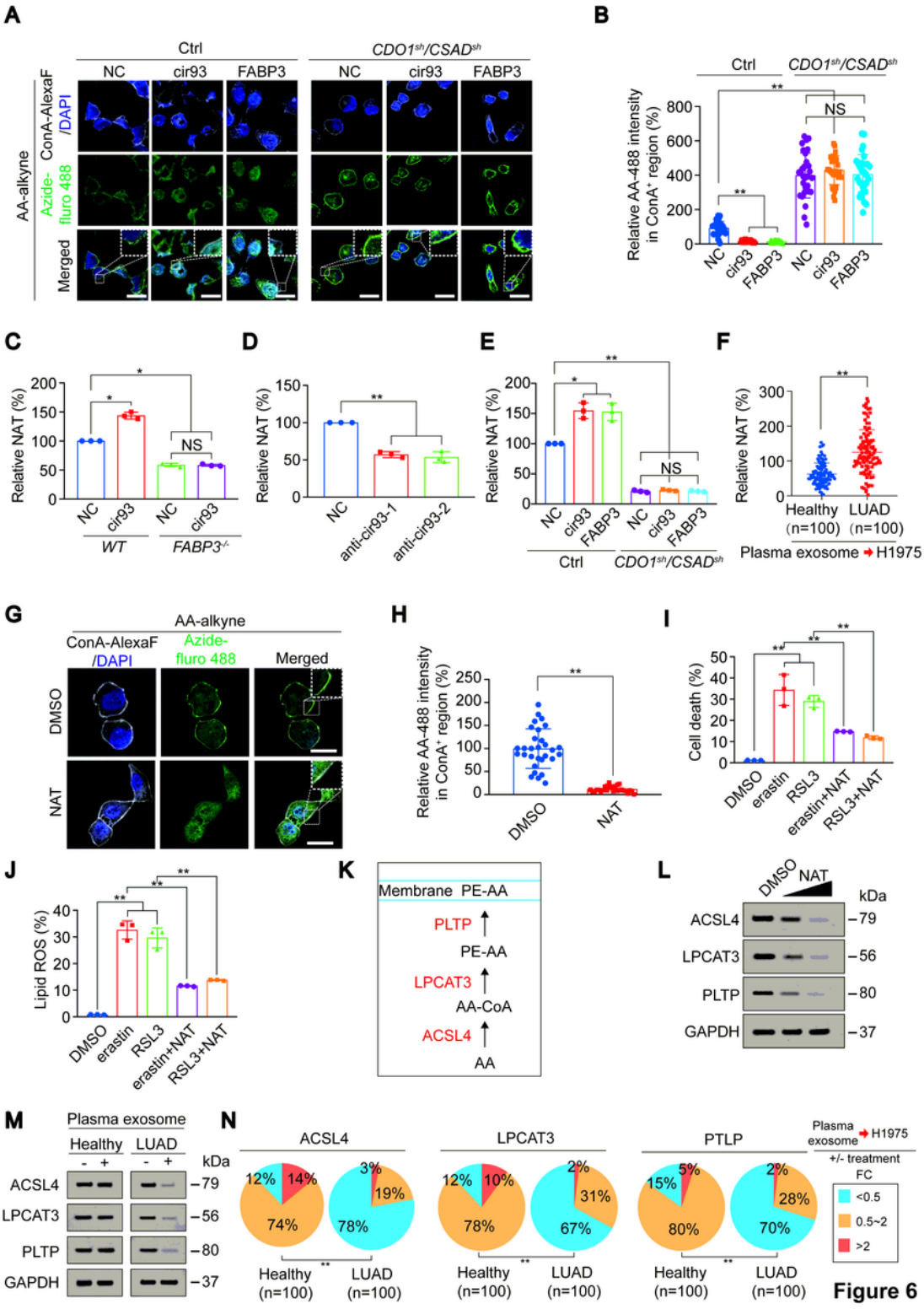

Figure 6

Figure 6

NAT suppressed AA incorporation into the plasma membrane. (A-B) AA incorporation into the plasma membrane, as measured by a click chemistry-based method in control and H1975 cells infected with shRNAs targeting against CDO1 and CSAD followed by overexpressing with or without cir93 or FABP3. The representative images are shown in panel A, and data were graphed in panel B. Scale bar, 50 μm. (C) NAT was measured in WT and FABP3-/- H1975 cells with or without overexpressing cir93. (D) NAT in

control and A549 cells treating with indicated anti-cir93. (E) NAT in control cells and H1975 cells infected with shRNAs targeting against CDO1 and CSAD followed by overexpressing with or without cir93 or FABP3. (F) NAT in H1975 cells following co-incubating plasma exosome from healthy individuals (n=100) and LUAD patients (n=100). (G-H) Incorporation of AA into plasma membrane in H1975 cells treated with DMSO or NAT (20 μM, 24h), as measured by a click chemistry-based method. Representative images are shown in panel G, and data were graphed in panel H. Scale bar, 20 μm. (I-J) Cell death (I) and lipid ROS generation (J) were measured in control cells and H1975 cells treated with erastin (10 μM, 16-24h) or RSL3 (5 μM, 16-24h) alone or in combination with NAT (20 μM, 16-24h). (K) Schematic presentation of how AA incorporates into the membrane and the enzymes involved. (L) Representative IB images of ACSL4, LPCAT3 and PLTP in H1975 cells treated with DMSO, or increasing concentration of NAT (10-20 μM, 24h). (M) Representative IB images of ACSL4, LPCAT3 and PLTP in H1975 cells following co-incubation of plasma exosome from healthy individuals or LUAD patients. (N) Percentages of the exosome from healthy individuals (n=100) and LUAD patients (n=100) for their effects to result in a different fold change (FC) of ACSL4, LPCAT3 and PTLP between the H1975 cells with or without co-incubation of plasma exosome. The data are shown as the mean ± SD from three biological replicates (including IB). *P < 0.05, **P < 0.01 indicates statistical significance. NS, non-significance. Data in B-E, I, J were analyzed using one-way ANOVA tests. Data in F, H were analyzed using student's t tests. Data in N were analyzed using a $\chi 2$ test.

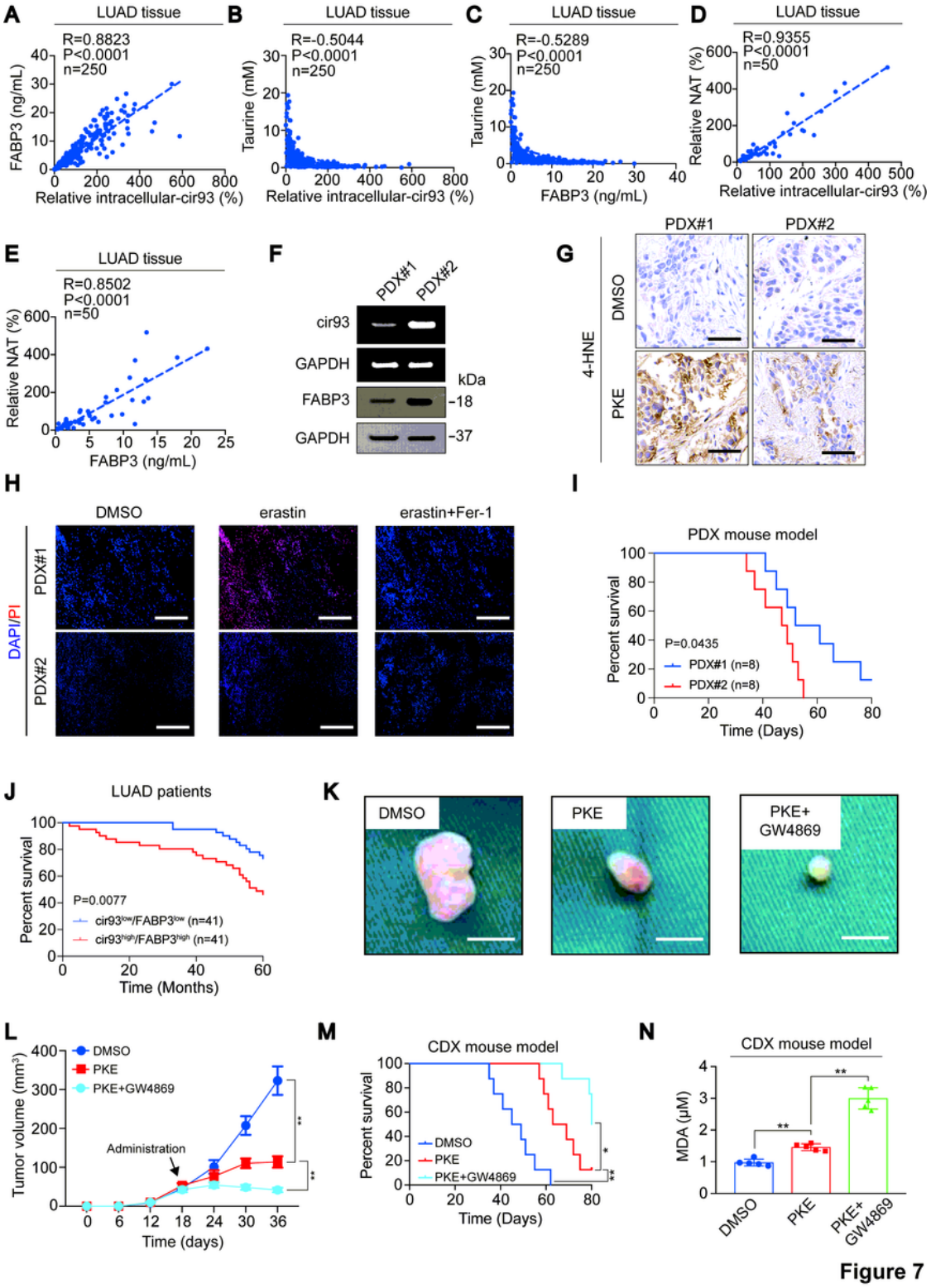

Figure 7

Figure 7

Clinical significance of the study. (A) Correlation between FABP3 and intracellular-cir93 in LUAD tissues (n=250). (B-C) The correlations between taurine and intracellular-cir93 (B, n=250) and between taurine and FABP3 (C, n=250) in LUAD tissues. (D-E) The correlations between NAT and intracellular-cir93 (D, n=50) and between NAT and FABP3 (E, n=50) in LUAD tissues. (F) Expression of cir93 and FABP3 in PDX#1 and PDX#2. (G) The levels of 4-HNE in PDX#1 and PDX#2 following administrating PKE

(20mg/kg, 2 weeks) in mice. Scale bar, 100 μm. (H) Tissue slices from PDX#1 and PDX#2 were treated with DMSO, erastin (10 μM, 24h), in the presence or absence of Fer-1 (1 μM, 24h) ex vivo, followed by staining with PI. Scale bar, 500 μm. (I) OS of PDX-bearing mice (n=8/group). (J) OS of LUAD patients with indicated cir93 and FABP3 expression levels (n=41/group). (K-L) Co-administrating GW4869 improved PKE efficacy in A549 cell-based CDX mouse models. Representative images of tumors at the end of experiment, in which mice were administrated with DMSO or PKE (20mg/kg), in the presence or absence of GW4869 (2mg/kg), are shown in panel K, and the tumor growth curves were graphed in panel L. Scale bar, 5 mm. (M) OS curves in A549 cell-based CDX mice following administrating with DMSO, PKE (20mg/kg, 3 weeks), in the presence or absence of GW4869 (2mg/kg, 3 weeks). (N) MDA concentrations in the tumors from panel K-L. The data are shown as the mean ± SD from three biological replicates (including IB). *P < 0.05, **P < 0.01 indicates statistical significance. Data in A-E were analyzed using Spearman rank-correlation analysis. Data in I, J, M were analyzed using log rank tests. Data in L were analyzed using a two-way ANOVA test. Data in N were analyzed using a one-way ANOVA test.

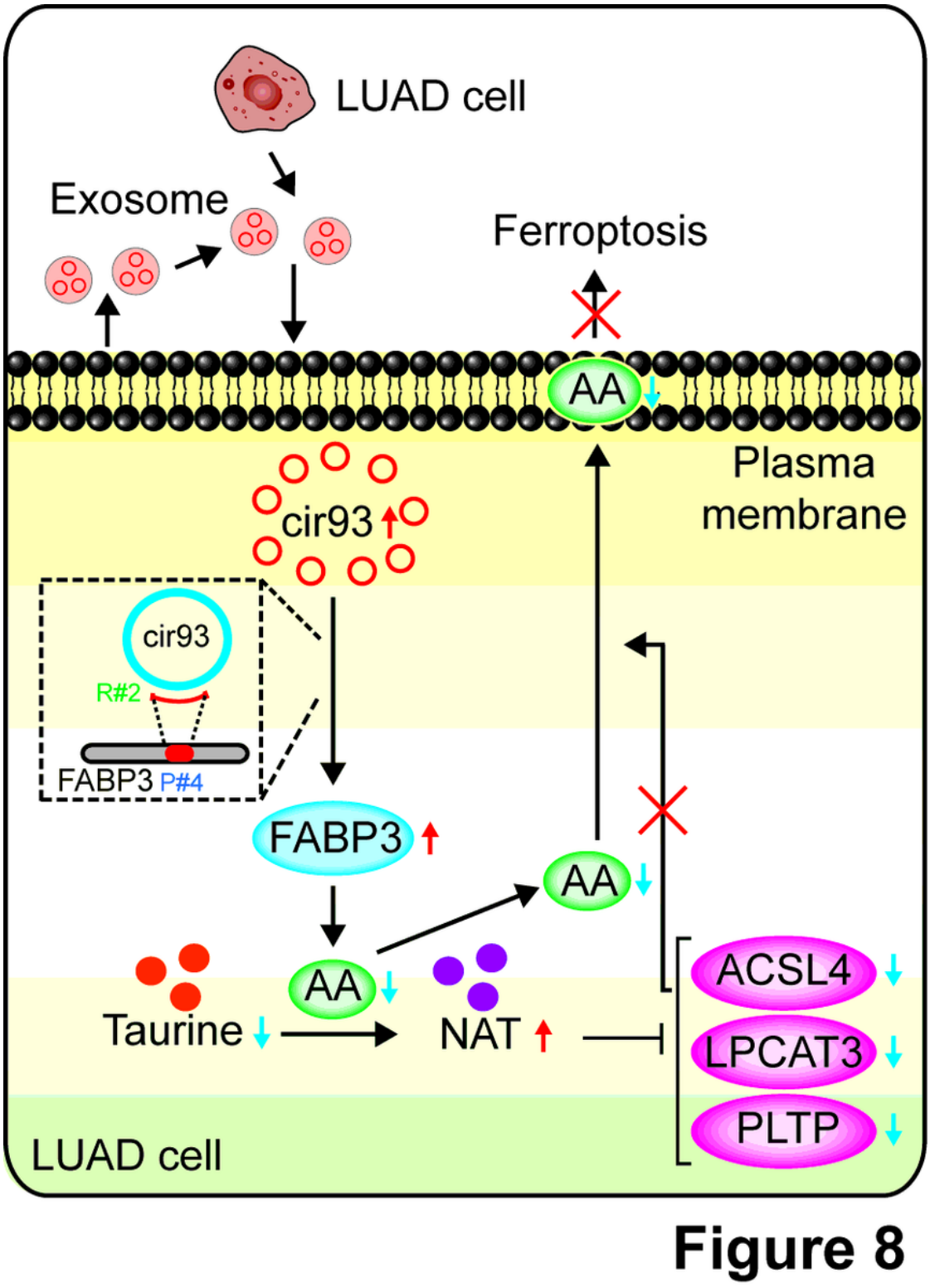

Figure 8

Figure 8

Schematic representation of the study. Briefly, exosome secreted by LUAD cells themselves is essential to elevate intracellular-cir93 in LUAD cells. The intracellular cir93-FABP3 interaction is critical to upregulate FABP3 for stimulating the reduction of global-AA via reaction with taurine. Besides, the function of NAT, the product of taurine and AA, to prevent AA incorporation into the plasma membrane via suppressing ACSL4, LPCAT3 and PLTP has also been uncovered in this study. Therefore, the roles of exosome and

cir93 to reduce lipid peroxidation and desensitize ferroptosis in LUAD cells are established and might be helpful to treat against LUAD in the future.

Supplementary Files

This is a list of supplementary files associated with this preprint. Click to download.

- SupplementaryFigures.pdf
- SupplementaryTables.pdf